



HAL
open science

Leptin, BMI, and a Metabolic Gene Expression Signature Associated with Clinical Outcome to VEGF Inhibition in Colorectal Cancer

Aurélien J C Pommier, Matthew Farren, Bhavika Patel, Mark Wappett, Filippou Michopoulos, Neil R Smith, Jane Kendrew, Jeremy Frith, Russell Huby, Catherine Eberlein, et al.

► **To cite this version:**

Aurélien J C Pommier, Matthew Farren, Bhavika Patel, Mark Wappett, Filippou Michopoulos, et al.. Leptin, BMI, and a Metabolic Gene Expression Signature Associated with Clinical Outcome to VEGF Inhibition in Colorectal Cancer. 2015, pp.77 - 93. 10.1016/j.cmet.2015.10.015 . hal-04622737

HAL Id: hal-04622737

<https://hal.science/hal-04622737>

Submitted on 24 Jun 2024

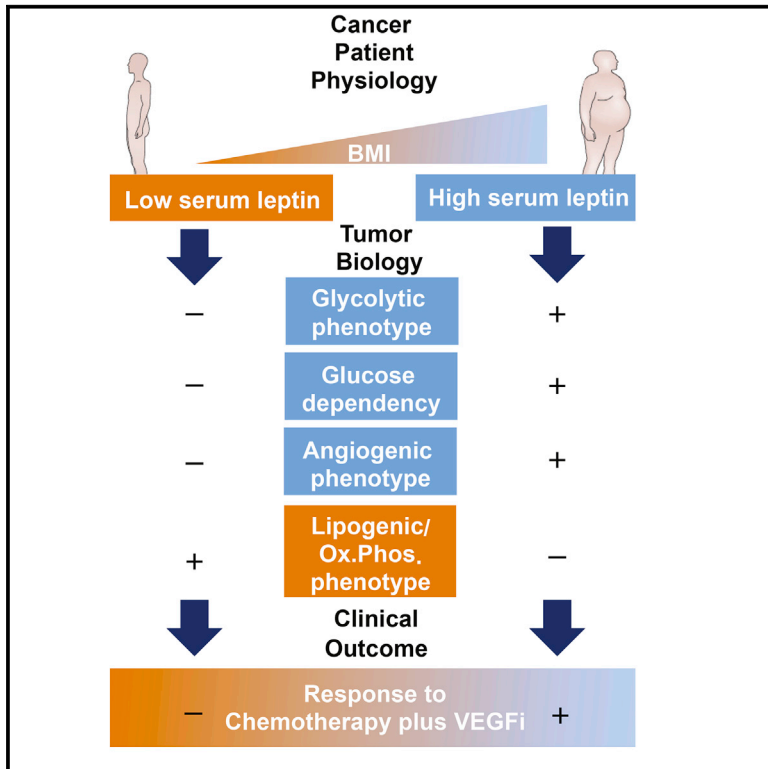
HAL is a multi-disciplinary open access archive for the deposit and dissemination of scientific research documents, whether they are published or not. The documents may come from teaching and research institutions in France or abroad, or from public or private research centers.

L'archive ouverte pluridisciplinaire **HAL**, est destinée au dépôt et à la diffusion de documents scientifiques de niveau recherche, publiés ou non, émanant des établissements d'enseignement et de recherche français ou étrangers, des laboratoires publics ou privés.

Cell Metabolism

Leptin, BMI, and a Metabolic Gene Expression Signature Associated with Clinical Outcome to VEGF Inhibition in Colorectal Cancer

Graphical Abstract



Authors

Aurélien J.C. Pommier,
Matthew Farren, Bhavika Patel, ...,
Shethah Morgan, Susan E. Critchlow,
Simon T. Barry

Correspondence

simon.t.barry@astrazeneca.com

In Brief

Response to VEGF signaling inhibitors is poorly understood. Pommier et al. revealed circulating leptin, BMI, and a tumor glycolytic/angiogenic/hypoxia profile associated with clinical response to VEGFR inhibition. Tumor cell metabolic profile also influenced sensitivity in pre-clinical models. The findings suggest that patient physiology and tumor cell phenotype may influence response to VEGFRi.

Highlights

- High circulating leptin and high BMI correlate with VEGFRi benefit in mCRC
- Tumors with greater response have a glycolytic/hypoxic/angiogenic phenotype
- Glycolytic/hypoxic/angiogenic phenotype influences preclinical VEGFRi sensitivity
- Leptin exposure induces a metabolic/angiogenic phenotype in cancer



Leptin, BMI, and a Metabolic Gene Expression Signature Associated with Clinical Outcome to VEGF Inhibition in Colorectal Cancer

Aurélien J.C. Pommier,^{1,2} Matthew Farren,³ Bhavika Patel,¹ Mark Wappett,¹ Filippos Michopoulos,¹ Neil R. Smith,¹ Jane Kendrew,¹ Jeremy Frith,¹ Russell Huby,¹ Catherine Eberlein,¹ Hayley Campbell,¹ Christopher Womack,¹ Paul D. Smith,¹ Jane Robertson,¹ Shethah Morgan,¹ Susan E. Critchlow,¹ and Simon T. Barry^{1,*}

¹AstraZeneca, Oncology iMED, Alderley Park, Macclesfield, Cheshire SK10 4TG, UK

²Centre d'Immunologie Pierre Fabre, 5 Avenue Napoléon III, 74160 Saint-Julien-en-Genevois, France

³Cancer Research Technology, Angel Building, St. John Street, London EC1V 4AD, UK

*Correspondence: simon.t.barry@astrazeneca.com

<http://dx.doi.org/10.1016/j.cmet.2015.10.015>

SUMMARY

VEGF (vascular endothelial growth factor) signaling inhibitors are widely used in different cancer types; however, patient selection remains a challenge. Analyses of samples from a phase III clinical trial in metastatic colorectal cancer testing chemotherapy versus chemotherapy with the small molecule VEGF receptors inhibitor cediranib identified circulating leptin levels, BMI, and a tumor metabolic and angiogenic gene expression signature associated with improved clinical outcome in patients treated with cediranib. Patients with a glycolytic and hypoxic/angiogenic profile were associated with increased benefit from cediranib, whereas patients with a high lipogenic, oxidative phosphorylation and serine biosynthesis signature did not gain benefit. These findings translated to pre-clinical tumor xenograft models where the same metabolic gene expression profiles were associated with *in vivo* sensitivity to cediranib as monotherapy. These findings suggest a link between patient physiology, tumor biology, and response to antiangiogenics, which may guide patient selection for VEGF therapy in the future.

INTRODUCTION

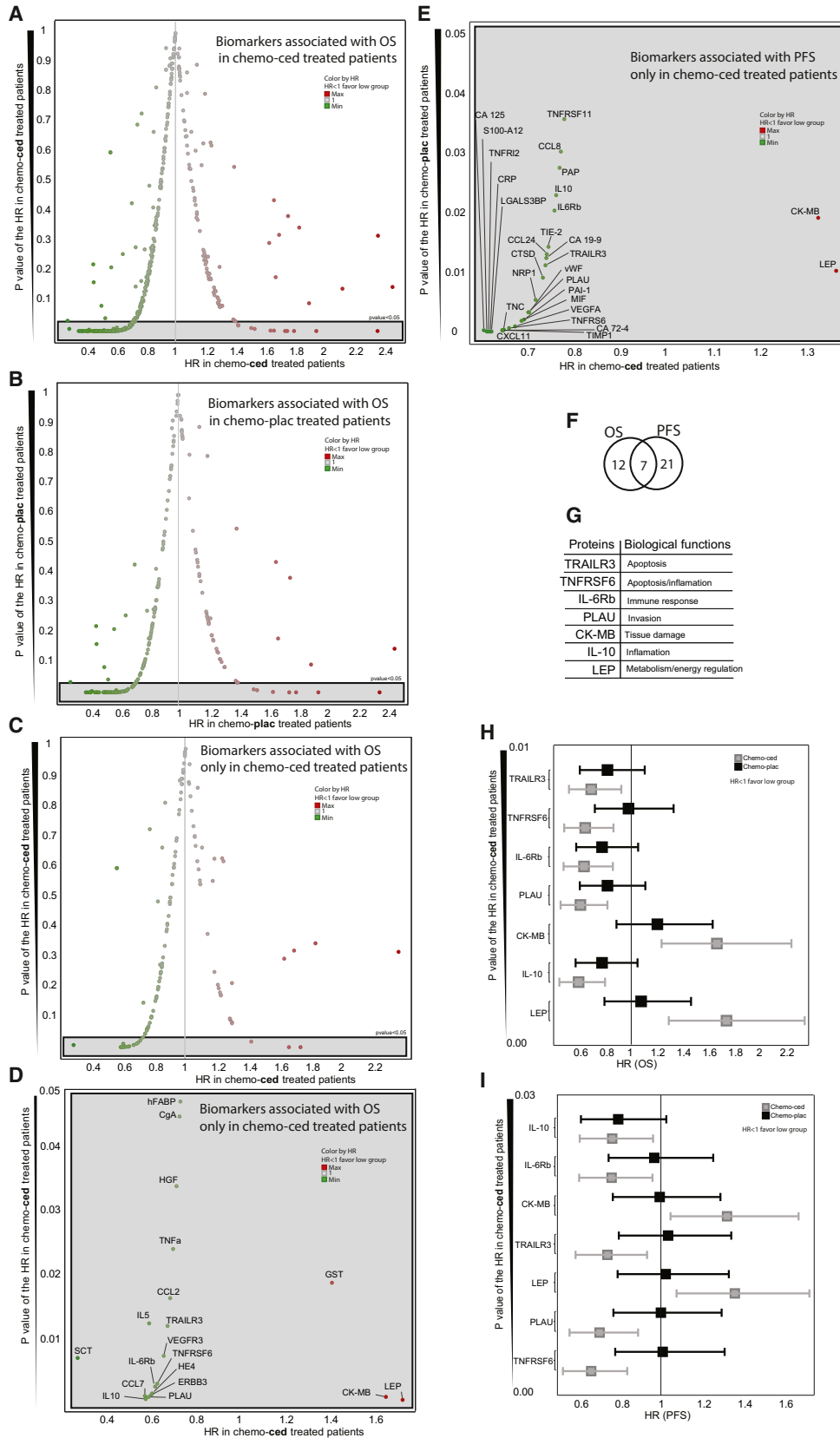
Angiogenesis plays an essential role in tumor growth and progression. Vascular endothelial growth factor (VEGF) is one of the key factors driving tumor angiogenesis. Many VEGF signaling inhibitors (VEGFi) have been tested clinically giving therapeutic benefit in a number of settings. Drugs targeting VEGF signaling pathways include: bevacizumab, a ligand-trapping monoclonal anti-VEGF antibody (Hurwitz et al., 2004); ramcicrimab, an antibody targeting VEGFR2 (Lu et al., 2002); cediranib and other oral small-molecule VEGFR tyrosine kinase inhibitors that target VEGFR-1, VEGFR-2, VEGFR-3, and c-Kit (Brave et al., 2011; Wedge et al., 2005).

While VEGF inhibitors give clinical benefit in a range of tumor settings, use in unselected patient populations has resulted in disappointing overall survival outcomes. To optimize the use of VEGF inhibitors, there is a need to identify biomarkers that predict benefit, and improvement in our understanding of factors affecting sensitivity. Several possible hypotheses (Bergers and Hanahan, 2008; Ellis and Hicklin, 2008) for intrinsic and acquired resistance to VEGF therapies have been investigated, mainly focused on the tumor micro-environment. These mechanisms include: upregulation of alternative pro-angiogenic signaling pathways such as PDGF-C (Crawford et al., 2009), FGF2 (Casanovas et al., 2005), SDF1 α (Xu et al., 2009), and DLL4 (Li et al., 2011); recruitment of vascular progenitor cells and pro-angiogenic monocytes from bone marrow (Shojaei and Ferrara, 2008; Shojaei et al., 2010; Shojaei et al., 2007) or T helper lymphocytes (Chung et al., 2013); increased protective coverage of tumor blood vessels by pericytes (Helfrich et al., 2010) and tumor-stromal architecture (Smith et al., 2013). However, none of these mechanisms have been adopted as a patient selection biomarker in the clinic.

The efficacy of cediranib plus FOLFOX/CAPOX (chemotherapy) versus placebo plus FOLFOX/CAPOX in patients with previously untreated metastatic colorectal cancer (mCRC) was assessed in the phase III HORIZON II trial (ClinicalTrials.gov identifier NCT00399035). This study met the co-primary endpoint of improved progression-free survival (PFS) with cediranib plus FOLFOX/CAPOX treatment, compared to FOLFOX/CAPOX alone. However, the primary endpoint of improved overall survival (OS) was not met, a common outcome for VEGF-targeting agents (Bergers and Hanahan, 2008; Casanovas et al., 2005; Jain et al., 2006).

Serum biomarkers can be used to identify patient subgroups that respond differently to VEGFi-based therapy (Tran et al., 2012). In the HORIZON II trial, several prognostic and pharmacodynamic serum biomarkers were identified (Pommier et al., 2014; Spencer et al., 2013). Biomarkers for the selection of treatment-sensitive patients, however, are yet to be discovered. To identify potential patient stratification biomarkers, we have determined the predictive value of multiple serum proteins and tumor genes using samples from patients enrolled in HORIZON II. We have explored the mechanistic relevance of selected markers in preclinical models.





(legend on next page)

RESULTS AND DISCUSSION

Baseline Serum Proteins Profiling Reveals Markers Associated with PFS and OS in mCRC Patients Treated with Chemo Plus Cediranib

The concentration of 207 serum proteins (Table S1) was determined for 582 mCRC patients enrolled in the phase III randomized double-blind HORIZON II trial of the VEGFi inhibitor cediranib (Hoff et al., 2012). Patients were treated with either chemotherapy plus cediranib 20 mg (chemo-ced) or chemotherapy plus placebo (chemo-plac). For each protein, patients were dichotomized into high and low categories based on the median baseline serum concentrations. Correlation with OS was determined using two separated Cox proportional hazard models, comparing sensitivity of patients (high versus low categories) in response to (1) chemo-ced (Figure 1A) and (2) chemo-plac treatment (Figure 1B). Hazard ratio (HR) and p value are represented as volcano plots for all of the serum proteins. Proteins demonstrating a significant HR ($p < 0.05$) are highlighted (gray box). To focus our analysis on the identification of biomarkers related with cediranib benefit (Figure 1C), we excluded the proteins that were already associated with OS in chemo-plac (Figure 1B) from the volcano plot in Figure 1A. This revealed a number of biomarkers significantly associated with OS in patients receiving chemo-ced but not chemo-plac (Figure 1D). The same approach identified several biomarkers correlated with PFS in response to chemo-ced (Figure 1E). Given a p value cutoff of 0.05, 5% of the biomarkers would be expected to be associated with PFS or OS by chance alone. To reduce this false-positive rate, we focused on proteins associated with both PFS and OS (Figure 1F). HR, confidence interval (CI), and p values are represented by the forest plots for OS (Figure 1H) and PFS (Figure 1I). Patients classified as having high serum concentrations of leptin (LEP) or creatine kinase muscle and brain (CK-MB) had longer PFS and OS than did those with low concentrations. Patients with low serum concentrations of interleukin 10 (IL-10), plasminogen activator urokinase (PLAUR), interleukin 6 receptor beta (IL6Rb), TNF receptor superfamily member 6 (TNFSF6), and TNF related apoptosis inducing ligand receptor 3 (TRAILR3) had longer PFS and OS than did those with high concentrations. Figure 1G summarizes the biological functions of these proteins.

High Serum Leptin Associated with Prolonged Overall Survival in Cediranib-Treated Patients with mCRC

The association between leptin concentrations and clinical outcome in cediranib-treated patients was of particular inter-

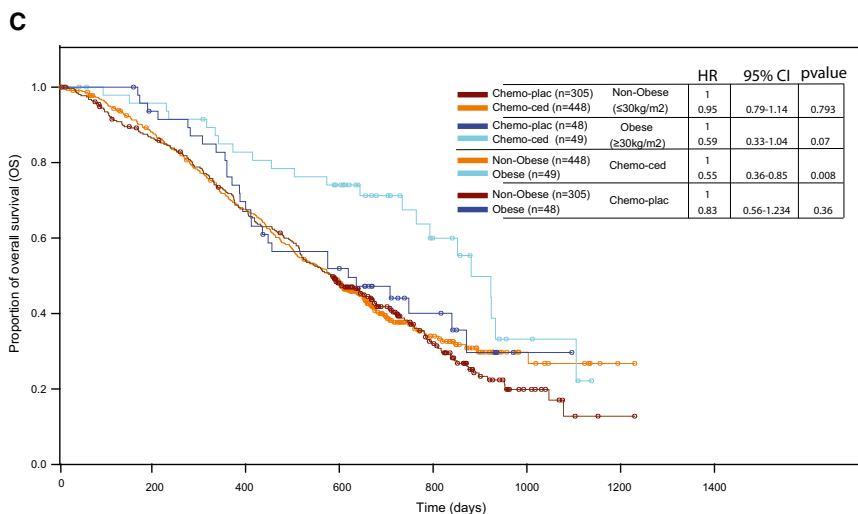
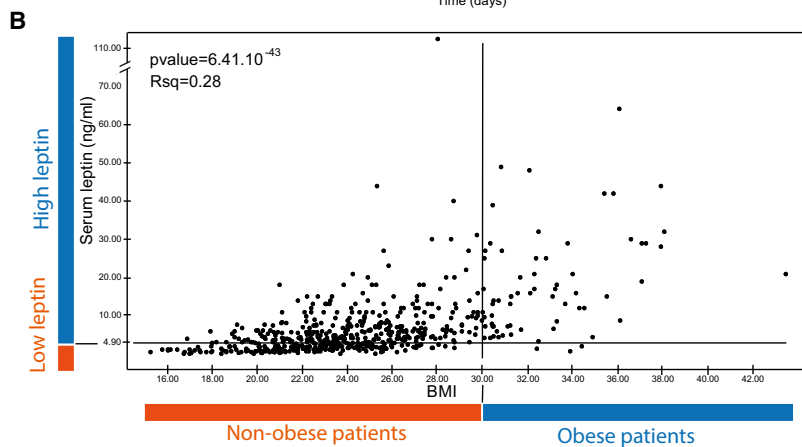
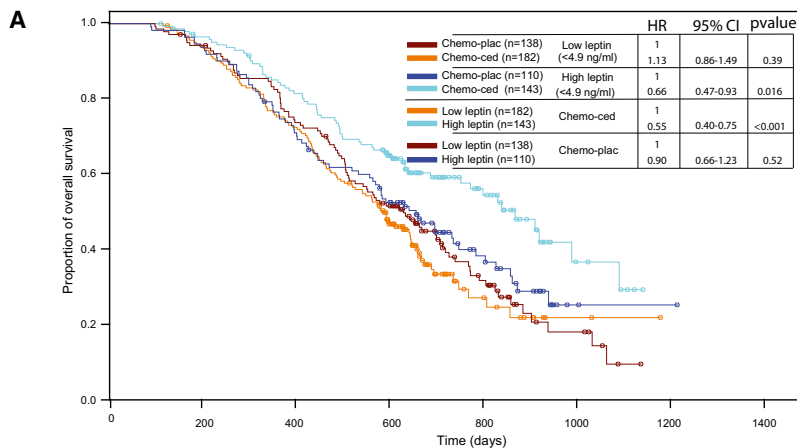
est for several reasons. First, leptin was the most significant protein associated with prolonged OS only in cediranib-treated patients (Figures 1D and 1H). Second, leptin has been shown to modify many aspects of tumor biology including angiogenesis (Park et al., 2001). Third, leptin is an adipokine strongly correlated with obesity; elevated levels increase the risk of developing many types of cancers including CRC (Garofalo and Surmacz, 2006; Vucenic and Stains, 2012). The impact of leptin status versus therapy on OS is represented by Kaplan-Meier curves, with HR, CI, and p values demonstrating significant differences between arms (Figure 2A). Interaction between treatments and leptin status was significant for OS ($p_{\text{interaction}} < 0.001$) and PFS ($p_{\text{interaction}} = 0.001$) (Figure S1A). Patients with high serum leptin concentration showed an improved OS in response to chemo-ced when compared to low leptin patients (HR = 0.55, CI = 0.40–0.75, $p < 0.001$), but also when compared to patients treated with chemo-plac (HR = 0.66, CI = 0.47–0.93, $p = 0.016$) (Figure 2A). Importantly, serum leptin concentration was not associated with OS in patients treated with chemo-plac (HR = 0.90, CI = 0.66–1.23, $p = 0.52$).

High circulating leptin is often associated with obesity (Widjaja et al., 1997). To determine whether obesity was linked with clinical response to cediranib, we correlated the BMI with leptin concentrations (Figure 2B) and BMI with overall survival (Figure 2C, $n = 859$ patients). BMI and serum leptin concentration were positively correlated in this cohort (Figure 2B). We found a significant interaction between obesity (as defined by a BMI ≥ 30 kg/m² by the current World Health Organization standard classification) and cediranib treatment on OS ($p_{\text{interaction}} = 0.024$) (Figure 2C) and PFS ($p_{\text{interaction}} = 0.028$) (Figure S1B). Obese patients were associated with prolonged OS in response to chemo-ced compared to non-obese patients (HR = 0.551, CI = 0.36–0.85, $p = 0.008$). However, in chemo-plac-treated patients, obesity was not associated with benefit on OS (HR = 0.831, CI = 0.56–1.234, $p = 0.359$).

Correlations between obesity measures and responsiveness to anti-angiogenic drugs have been reported elsewhere. The predictive value of visceral fat area (VFA) or surface body area measures are variable. Both are predictive of PFS and OS benefit from VEGFi TKI in metastatic clear cell renal cancer (Steffens et al., 2011), though neither is associated with response to bevacizumab in patients with CRC (Guu et al., 2010; Simkens et al., 2011). While there isn't a clear consensus, the majority of studies

Figure 1. Identification of Serum Biomarkers Associated with Clinical Outcome in Metastatic Colorectal Cancer Patients Related to Chemo-therapy Plus Cediranib

The concentrations of 207 serum proteins were measured by multiplex analyses in 582 patients with metastatic colorectal cancer. Each quantified protein is represented as a dot. For each protein, patients were dichotomized into high and low categories based on the median baseline serum concentrations. (A and B) Cox regression models were used to compare overall survival (OS) of patients (high versus low categories) in response to chemo-ced (A) and chemo-plac treatment (B). Hazard ratio (HR) and p values (Cox regression model) associated with these analyses are represented by the volcano plots for all the serum proteins. The proteins showing a significant ($p < 0.05$) HR are highlighted in gray. (C and D) These volcano plots show the proteins only associated with OS in patients treated with cediranib (C). Proteins found already associated with response to chemo-plac were excluded in these plots. A magnification on the proteins found with a $p < 0.05$ is shown (D). (E) Identical analyses led to the identification of serum proteins correlated with progression-free survival (PFS) only in patients treated with chemo-ced. (F) Venn diagram highlighting the number of proteins associated with PFS and OS, PFS exclusively and OS exclusively in patients treated with chemo-ced. (G) Main biological functions of the proteins found associated with PFS and OS. (H and I) Forest plots (HR and confident interval) show the impact of serum concentrations and treatments on OS (H) and PFS (I). Full names of the analyzed proteins are detailed in Table S1.



suggest high leptin concentrations and obesity are associated with a higher risk of colon cancer, and possibly poor outcome (Larsson and Wolk, 2007; Ma et al., 2013). Our data suggest that circulating leptin levels are a surrogate measure for BMI and may be associated with improved clinical outcomes in mCRC patients receiving VEGFi-based therapy. It will be important to consider which of these features associate with outcome in other tumor types.

were stratified into two groups for each gene based on high and low gene expression (relative to median) and the OS and PFS compared in the patients treated with chemo-plac versus chemo-ced using a Cox regression model. The genes significantly associated with OS (Figure 3) and PFS (Figure S2C) are listed on the forest plots showing the HR, CI, and p values. Overall, high expression of genes involved in glucose metabolism, angiogenesis, hypoxia, glutamine metabolism, and

Figure 2. High Serum Leptin Concentrations and Obesity Improve Overall Survival of Patients Treated with Chemotherapy Plus Cediranib

(A) Kaplan-Meier analyses showing the impact of high versus low serum concentration of leptin and overall survival (OS) in response to chemotherapy ± cediranib.

(B) Linear regression analysis showing the correlation between serum concentrations and body mass index (BMI) in HORIZON II trial.

(C) Kaplan-Meier curves showing the impact of obesity (defined as BMI > 30) on OS in response to chemotherapy ± cediranib.

HR, hazard ratio; CI, confidence interval.

Baseline Tumor mRNA Profiling Reveals Genes Associated with Longer Survival in mCRC Patients Treated with Cediranib

Aerobic glycolysis and angiogenesis are important enablers of tumor progression (Hanahan and Weinberg, 2011). Given the association of leptin with metabolism and angiogenesis (Park et al., 2001, 2010; Yehuda-Shnaidman et al., 2013), we explored the relationship between the expression of genes involved in angiogenesis and tumor metabolism (Table S2) and clinical response in HORIZON II (Figure 3A). Viable tumor area from 354 available formalin-fixed diagnostic biopsies (Figure S2A) were marked and macro-dissected, excluding gross necrotic regions or non-tumor tissue, and RNA extracted (Figure S2B). 95 samples were excluded due to poor tissue quality, lack of tumor content, or low RNA yield/quality (Figure S2A). Gene expression was analyzed in 259 samples representing 26.5% of the patients treated with chemotherapy plus placebo (n = 95/358), 21.1% of the patients treated with chemotherapy plus cediranib 20 mg (n = 106/502), and 26.9% of the patients treated with chemotherapy plus cediranib 30 mg (n = 58/216) (Figure S2A).

We used two statistical analysis strategies to identify genes potentially predictive for response to cediranib. Patients

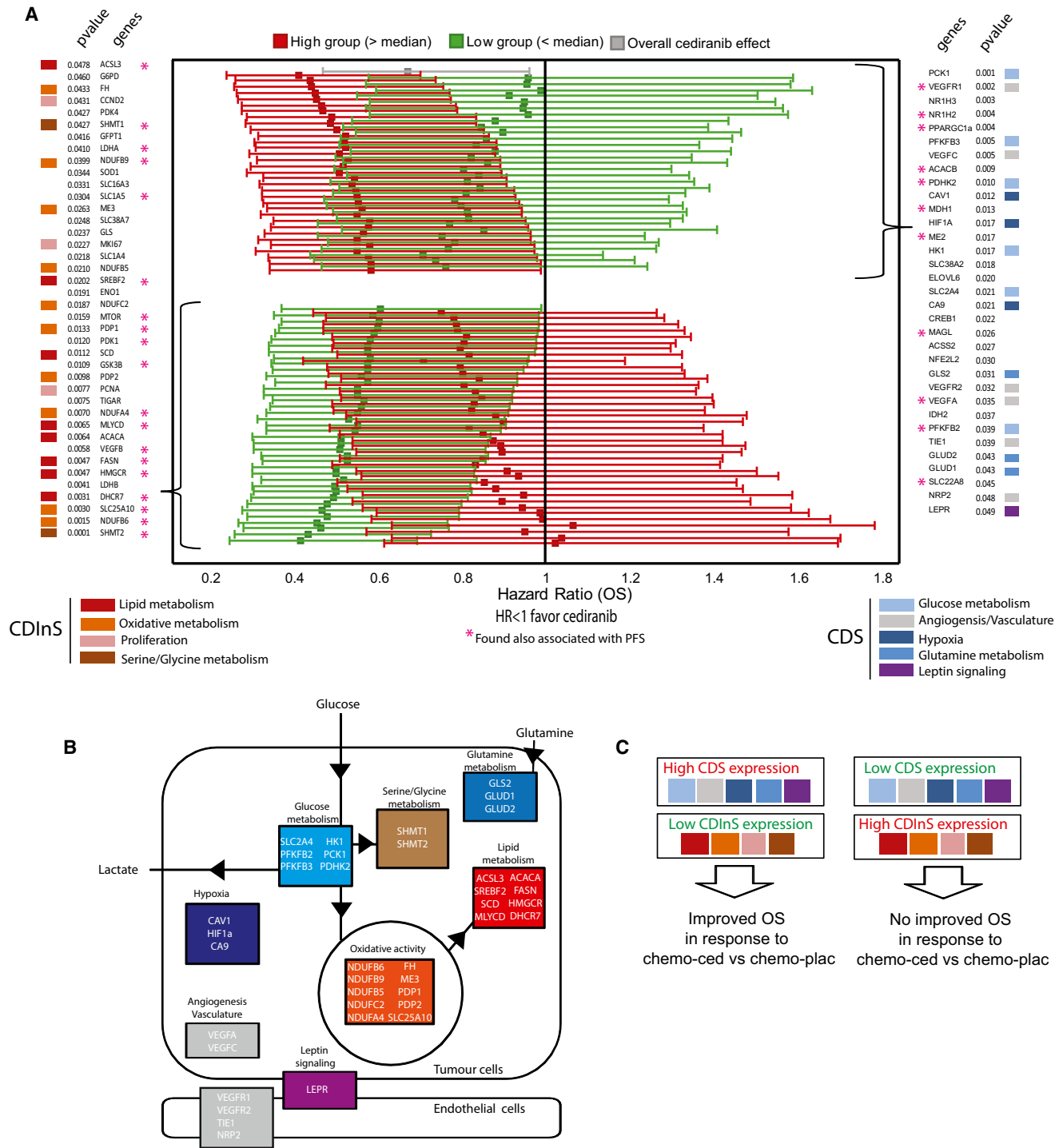


Figure 3. Expression of Genes Involved in Key Tumor Metabolic Pathways Is Associated with the Clinical Outcome Benefit of Cediranib in Metastatic Colorectal Cancer Patients

Baseline gene expression was quantified from diagnostic fixed formalin colorectal cancer biopsies using NanoString technology.

(A) The forest plot represents the impact of treatment (chemotherapy plus placebo versus chemotherapy plus cediranib) in patient groups defined as high and low expression (relative to the median for each gene) on overall survival (OS) for the significant genes ($p < 0.05$). The biological functions of the genes are shown by a color code. Pink stars indicate the genes also found associated with chemotherapy plus cediranib benefit on progression-free survival (PFS) (Figure S2C).

(B) Diagram representing the genes associated with cediranib sensitivity (CDS)/cediranib insensitivity (CDInS) and associated with OS benefit on chemotherapy plus cediranib compared to chemotherapy plus placebo treatment.

(C) Model summarizing the association between the expression of CDS/CDInS genes and OS benefit in response to chemotherapy plus cediranib.

HR, hazard ratio; CI, confidence interval.

leptin signaling (cediranib-sensitive signature [CDS]) correlated with an improved OS in patients treated with chemo-ced compared to chemo-plac (Figure 3A). However, low expression of genes involved in lipid metabolism, oxidative activity, proliferation, and serine synthesis (cediranib-insensitive signature [CDInS]) associated with improved survival in patients treated with chemo-ced compared with chemo-plac. Many of these genes (pink stars) were also found to be associated with PFS as illustrated by Venn diagrams (Figures S2D and S2E). Figures 3B and 3C summarize the biological pathways/genes associated with improved OS in response to chemo-ced.

Hierarchical clustering identified groups of genes associated with differential response to chemotherapy \pm cediranib. This stratified the mCRC patient population based on sub-clusters of co-expressed genes involved in common biological functions (Figures S3A–S3C). Two clusters of genes associated with cediranib sensitivity (Figure 4A) and cediranib insensitivity (Figure 4D) were identified that impacted OS (Figures 4B, 4C, 4E, and 4F) and PFS (Figure S5) in response to chemotherapy \pm cediranib. Importantly, independent of the treatments received, these signatures were not prognostic on OS (Figures 4B and 4E). However, we found a significant interaction between treatment effects and cediranib-sensitive ($p_{\text{interaction}} = 0.028$) and cediranib-insensitive ($p_{\text{interaction}} = 0.002$) signatures on OS (Figures 4C and 4F). These data indicate that patients with high expression of the cediranib-sensitive gene signature showed improved OS in response to cediranib addition to chemotherapy when compared to chemotherapy plus placebo (HR = 0.50; CI = 0.30–0.83, $p = 0.007$). No benefit on OS was observed in response to cediranib treatment in patients with low expression of this signature (HR = 1.03; CI = 0.62–1.71, $p = 0.900$). The cediranib-sensitive signature (CDS) was not associated with PFS benefit ($p_{\text{interaction}} = 0.204$; Figure S3D). A significant interaction between treatment effects and the cediranib-insensitive signature (CDInS) ($p = 0.002$) was observed (Figure 4F). Patients with low gene expression of this signature showed improved OS in response to chemo-ced (Figure 4F), particularly when compared to patients treated with chemotherapy plus placebo (HR = 0.42; CI = 0.26–0.68, $p < 0.001$). The cediranib-sensitive signature (CDS) was also predictive on PFS ($p_{\text{interaction}} = 0.026$; Figure S3E).

To explore the link between leptin and the metabolic gene profile of tumors, the correlation of baseline circulating leptin concentrations with tumor metabolic gene expression data from the HORIZON II clinical trial was determined. The patient population was stratified into two groups, high versus low, based on the median leptin serum level observed in the cohort (4.9 ng/ml). Patients with high circulating leptin concentrations express higher levels of hypoxic/glycolytic genes (*CA-9*, *SLC16A3*, *HIF1 α*) and lower levels of *PDP1* and *SLC16A1* than those with low leptin concentration (Figure 4G). A similar correlation between leptin, LEPR, and HIF1 α staining in CRC has been observed previously (Koda et al., 2007a). Leptin receptor (LEPR) is expressed on both tumor and endothelial cells (Bouloumié et al., 1998; Koda et al., 2007b; Wang et al., 2012); however, the major impact of leptin was associated with the tumor cells. In our study there was no correlation between serum leptin concentrations and the expression of mRNA biomarkers of vasculature in clinical samples.

In addition to the metabolism genes, the cediranib-sensitive signature associated with OS also included *VEGFR1*, *VEGFR2*, *NRP2*, and *VEGF-A* (Figures 3 and S2). *VEGFR1* gene expression (Wilson et al., 2013) and a VEGF-dependent vasculature gene signature (including *VEGFR1*, *VEGFR2*, *VEGFR3*, *NRP1*, and *NRP2*) associated with better outcomes in mCRC treated with bevacizumab-containing therapies (Brauer et al., 2013). The association between the angiogenic genes and the metabolic genes is interesting and warrants further investigation. The cancer glycolytic phenotype is also influenced by other factors such as upregulation of HIF1 α or mutation/deletion of *VHL*. These additional biomarkers should also be considered as we seek to understand drivers of VEGFi sensitivity. Overall, our data show that baseline expression of genes involved in angiogenesis and tumor metabolism can segregate mCRC patients into subgroups that may predict response to cediranib-based therapy.

Glucose, Serine, and Lipid Metabolism Gene Expression Correlates with Sensitivity to Cediranib in Xenograft Models

The association between baseline expression of genes associated with metabolism and clinical responsiveness to cediranib suggests that the metabolic phenotype of the tumor may determine sensitivity/resistance to VEGFi. This was investigated using pre-clinical models. The mRNA expression of genes involved in metabolism and proliferation using TaqMan assays (Table S3) was determined across 13 xenograft models (Figure S4G). To focus specifically on the tumor cells, only human transcripts were assessed. Individual genes associated with sensitivity to monotherapy cediranib across 13 models were determined by linear regression analysis (Figure 5A). Tumor growth inhibition (TGI) after approximately 20 days of 3 mg/kg/day cediranib treatment was greatest in the A498 clear cell renal carcinoma (ccRCC) model, which exhibited tumor regression (TGI = 112%). NCI-H526, a small cell lung cancer model, was the least sensitive with an average of 35% TGI. Examples of cediranib efficacy are shown for the NCI-H526, Lovo, SW620, and A498 models (Figure 5B). The expression of genes known to be associated with a glycolytic phenotype, namely *SLC16A3*, *CA-9*, *MYC*, *PKM2*, *PGAM1*, *SLC2A1*, *EPAS1*, and *LDHA* were positively and significantly ($p < 0.05$) correlated with sensitivity to cediranib (Figure 5A). However, high expression of genes involved in serine metabolism (*PHGDH*) and lipid metabolism (*ME2*, *SREBF2*, *ME3*, and *FASN*) was associated with a lack of response to cediranib. No correlation between mutation status and sensitivity to cediranib was found for *VHL*, *PTEN*, *PIK3CA*, *KRAS*, and *MYC* (Figure 5A).

The activation of the glycolytic pathway in xenograft models highly sensitive to cediranib treatment was confirmed by mass spectrometric metabolomic analyses of in vivo tumor samples (Figure 5C). We found higher fructose-6-phosphate levels and lower NADPH levels in highly sensitive models (786-O, SW620, A498) compared with less sensitive models (NCI-H526, HCT-15, Calu-6, Lovo), consistent with the metabolic gene expression profile of the cediranib-sensitive versus cediranib-insensitive clinical samples.

Similar reductions in micro-vessel density (MVD) occurred in NCI-H526 and Lovo versus SW620 xenografts (Figure 5D), suggesting this does not contribute to the efficacy of cediranib.

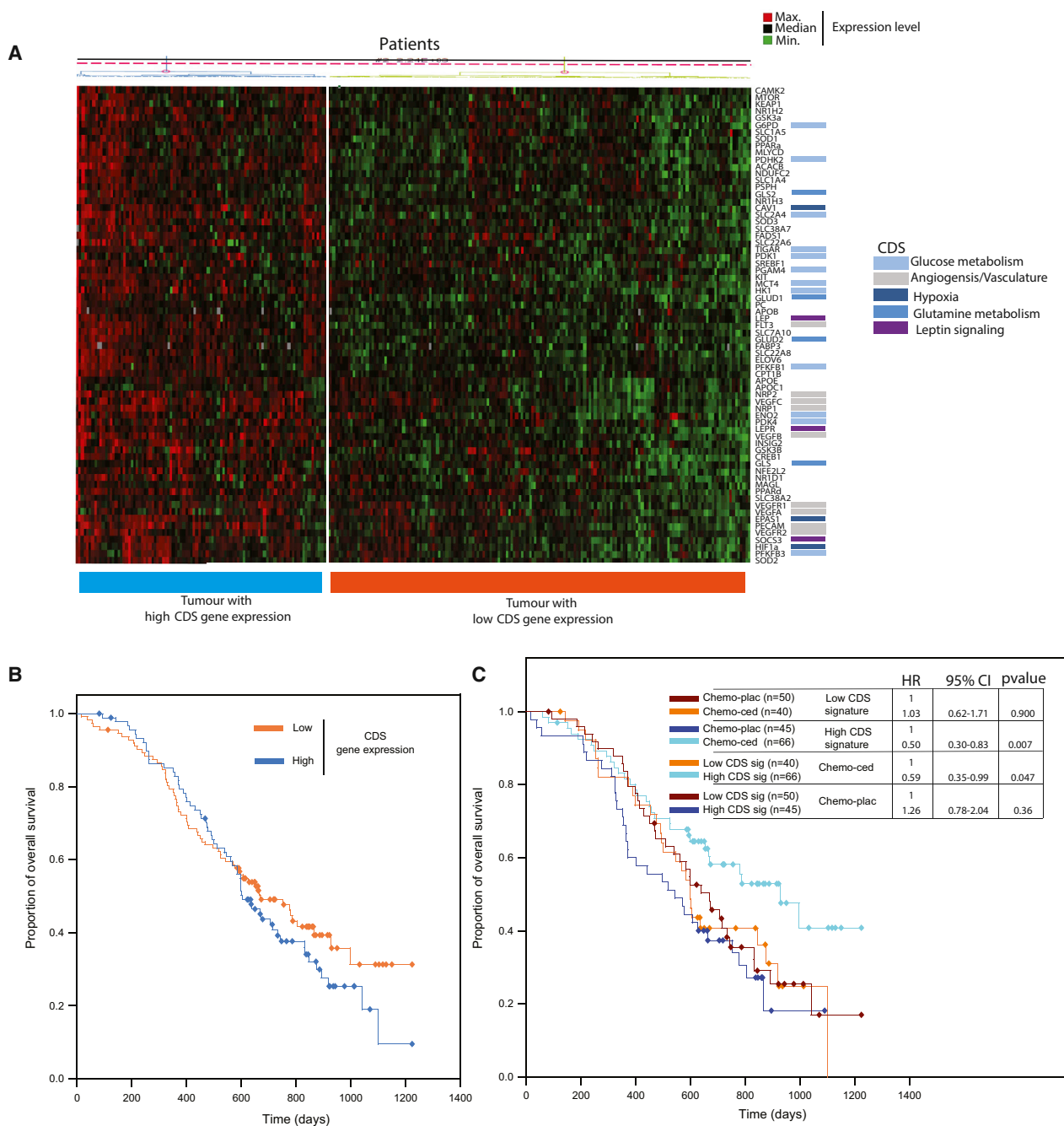


Figure 4. Expression Signatures of Genes Involved in Key Tumor Metabolic Pathways Predict Overall Survival Benefit in Metastatic Colorectal Cancer Patients Treated with Chemotherapy Plus Cediranib

(A) Stratification of the patients based on hierarchical clustering of co-expressed genes associated with cediranib sensitivity (CDS).

(B) Comparison of the overall survival (OS) in patients with high and low expression CDS genes showing the absence of prognostic value of this signature independently of treatments.

(C) Kaplan-Meier curves and Cox regression analyses comparing the effect of chemotherapy plus placebo and chemotherapy plus cediranib in patients with high and low CDS gene expression on OS.

(D) Stratification of the patients based on hierarchical clustering of co-expressed genes associated with cediranib insensitivity (CDInS) genes.

(E) Comparison of the OS in patients with high and low expression of CDInS genes showing the absence of prognostic value of this signature independently of treatments.

(F) Kaplan-Meier curves and Cox regression analyses comparing the effect of chemo-plac and chemo-ced in patients with high and low CDInS expression on OS.

(G) Genes correlated with serum leptin concentration were quantified in patients from HORIZON II clinical trial. Patient groups with high versus low leptin concentrations were determined based on the median concentration (4.9 ng/ml).

p values were determined by a Mann-Whitney test, and $p < 0.05$ was considered significant.

(figure continued on next page)

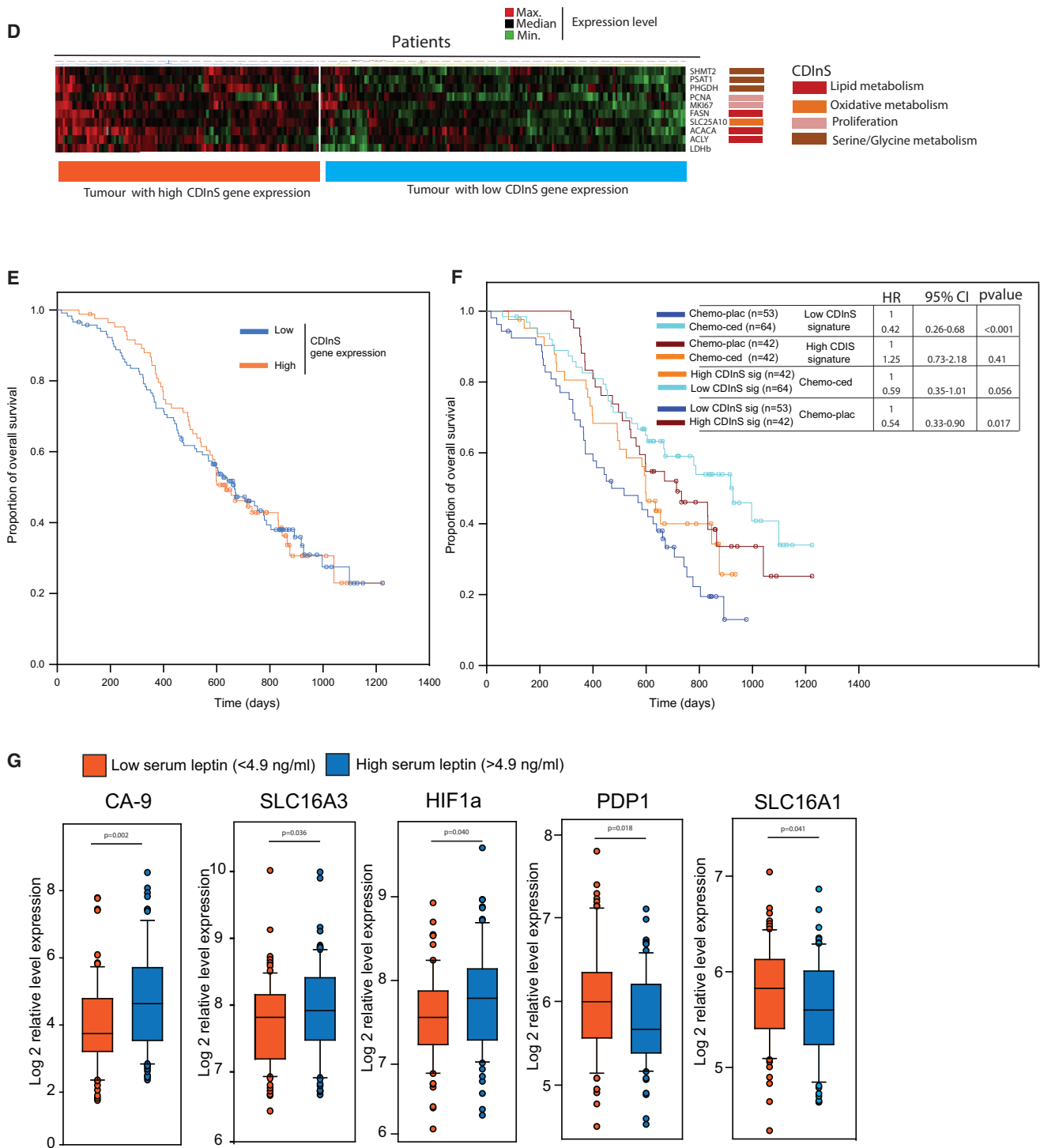


Figure 4. Continued

Consistently, tumor progression in the absence of re-vascularization has been described as a mechanism of escape after cediranib therapy in GBM (di Tomaso et al., 2011).

Raised expression of glycolytic enzymes and a corresponding increased sensitivity to VEGFi has been observed in xenografts

(Nardo et al., 2011) and in the clinic (Koukourakis et al., 2011; Wilson et al., 2013). Tumors display a range of metabolic phenotypes, some more dependent on the glycolytic pathway, others on mitochondrial oxidative activity (Zheng, 2012). The latter is likely to favor tumor growth following changes in vasculature

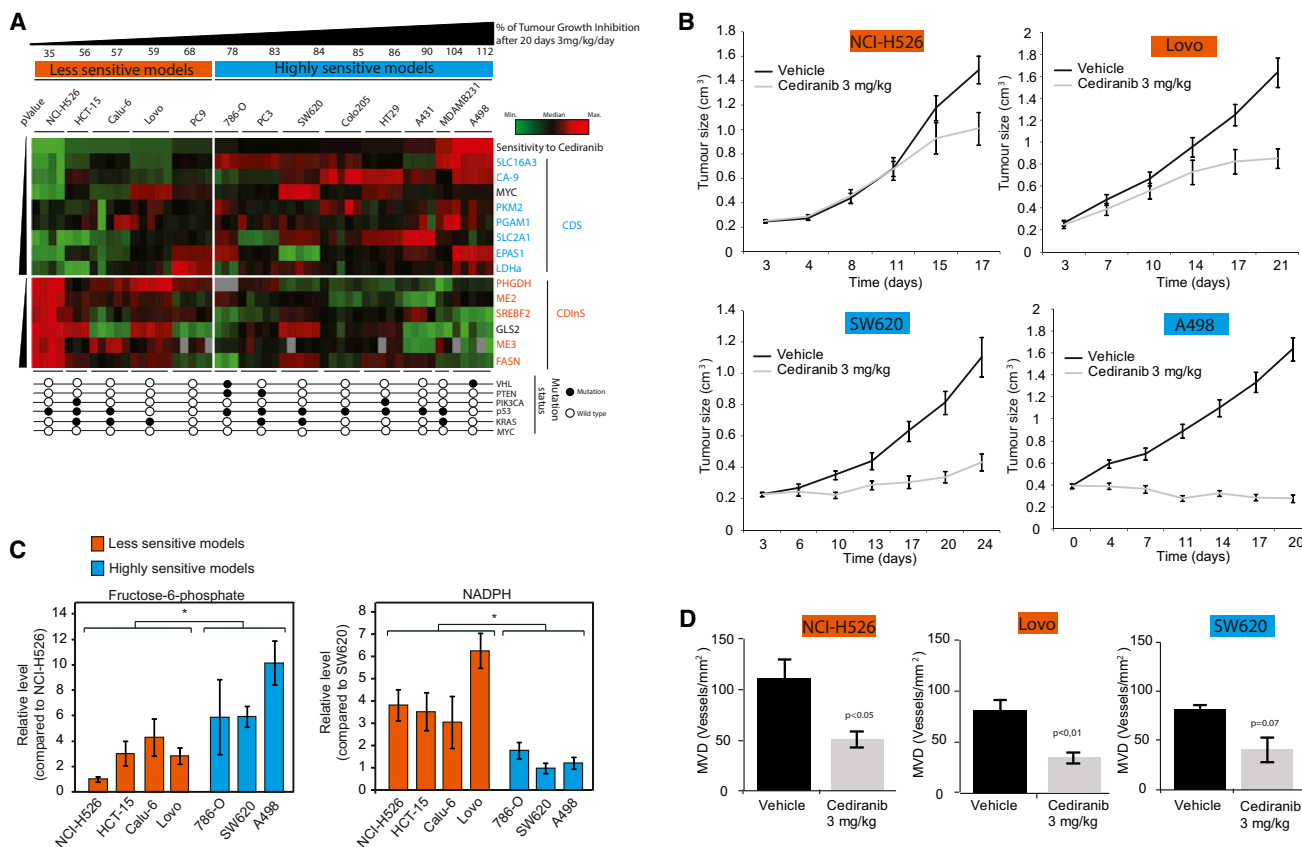


Figure 5. Glycolytic Phenotype Correlates with Sensitivity to Cediranib in Xenograft Models

(A) Human (tumor-derived) genes significantly correlated with sensitivity to cediranib in xenograft models are represented. The heatmap shows the relative expression level for each gene across the 13 xenografts. Each square represents a biological sample. Sensitivity to cediranib was determined by the tumor growth inhibition after 20 (± 3) days of cediranib treatment at 3 mg/kg/day. The average gene expression for each individual model ($n = 3-5$ animals) was correlated with sensitivity to cediranib by linear regression. $p < 0.05$ was considered significant. Mutation status for *VHL*, *PTEN*, *PIK3CA*, *TP53*, *KRAS*, and *MYC* is shown.

(B) Examples of cediranib efficacy is shown for NCI-H526, LoVo, SW620, and A498. Error bars represent SD of 6–10 biological replicates.

(C) The level of fructose-6-phosphate and NADPH were quantified *in vivo* in less- and highly sensitive models to cediranib. For each metabolite, levels were averaged ($n = 5-6$ animal per model). p values were determined by a t test comparison between less- and highly sensitive models. Error bars represent SD of 5 biological replicates.

(D) Effect of cediranib treatment on micro vessels density (MVD) in NCH-H526, LoVo, and SW620. Error bars represent SD of 5 biological replicates. p values were determined by a t test comparison, and $p < 0.05$ was considered significant. CDS, cediranib sensitive; CDInS, cediranib insensitive.

that decrease blood flow and vascular permeability (Bokacheva et al., 2013), limit the supply of nutrients and oxygen (Ebos et al., 2009), and restrict levels of glucose and ATP (Nardo et al., 2011). Dependency on the glycolytic pathway may render a cell more sensitive to these changes, as supply of glycolytic intermediates is critical for biomass production and proliferation (Vander Heiden et al., 2011). However, efficient utilization of nutrients or elevation of *de novo* biosynthetic pathways could enable adaptation to VEGFi treatment. High expression of *FASN* (Swinnen et al., 2002), *PHGDH* (Locasale et al., 2011; Possemato et al., 2011), and *SHMT2* (Jain et al., 2012) supporting lipid, serine, and glycine synthesis in tumor cells with low glycolytic activity may favor tumor survival.

Taken together, the data are consistent with the hypothesis that the intrinsic tumor metabolic phenotype affects responsiveness to cediranib, with a glycolytic phenotype associated with high sensitivity to cediranib. Conversely, low activity of the glyco-

lytic pathway and high expression of genes involved in serine synthesis and lipid biosynthesis is associated with lack of responsiveness to cediranib.

Changes in Hypoxic and Metabolic Gene Expression following Cediranib Treatment

Given that sensitivity to cediranib is in part endowed by a glycolytic gene expression profile, using gene expression profiling we investigated whether xenografts adapt to cediranib treatment and whether such adaptation depends on the sensitivity of the xenografts to cediranib (Figure S4). Although a large number of genes changed on cediranib treatment, the amplitudes of the changes were relatively small. The most consistent change was increased expression of several glycolytic/hypoxic genes (including CA-9), upregulated in the less-sensitive xenografts NCI-H526 and Calu-6 (Figures S4D and S4E). This suggests that cediranib causes hypoxia in these tumors, inducing the

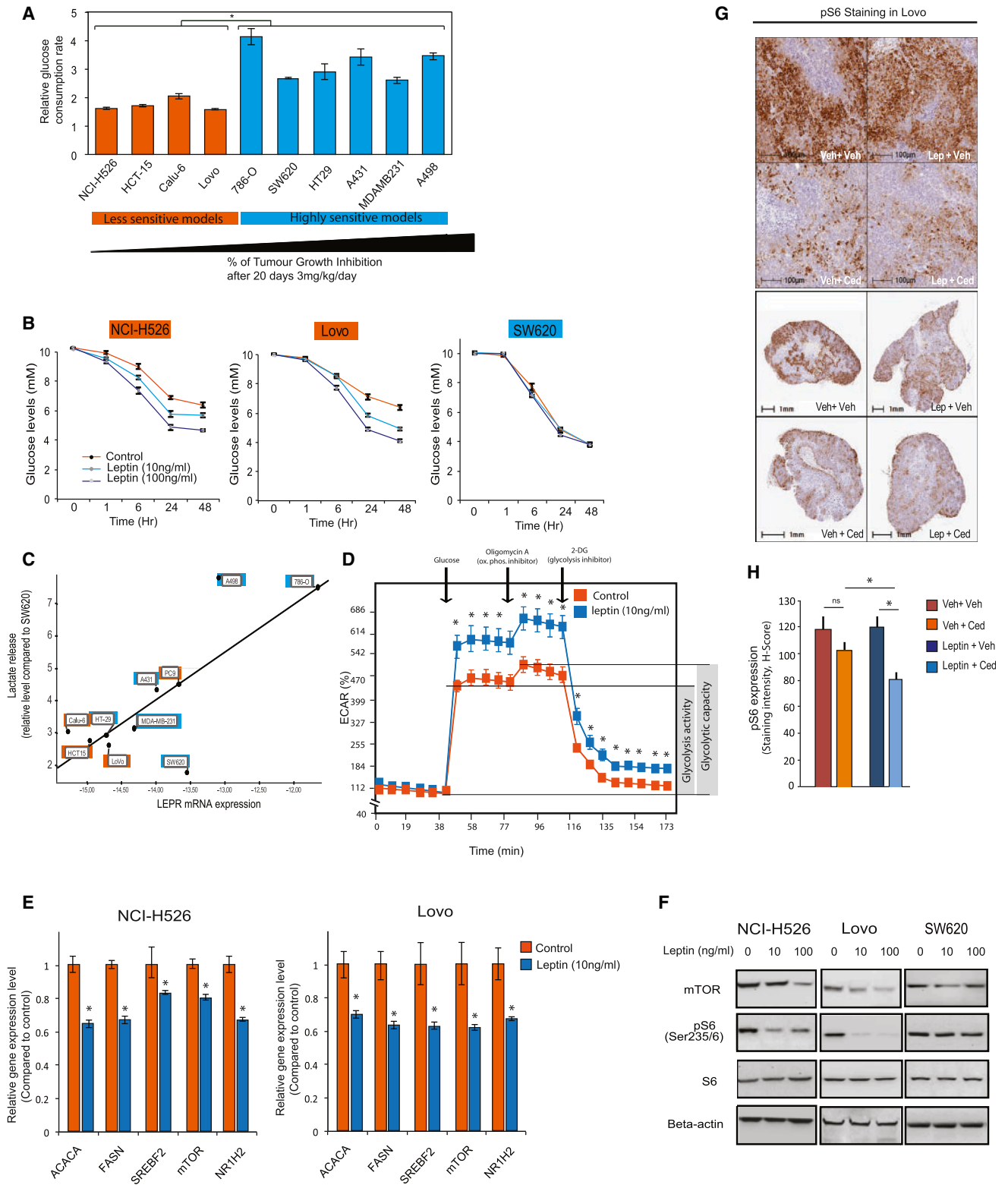


Figure 6. Leptin Modulates Tumor Metabolic Phenotype

(A) In vitro relative glucose consumption rate is compared between less- and highly sensitive models to cediranib. Error bars represent SD of 3 biological replicates.

(B) Kinetics of glucose consumption in cancer cells treated with increasing doses of leptin. Error bars represent SD of 3 biological replicates.

(C) Correlation between LEPR expression and lactate release in a panel of in vitro cell lines.

(legend continued on next page)

observed changes in gene expression. This did not occur in the highly sensitive A498, SW620, and 786-O models, despite a significant reduction in tumor vessel density following treatment. Consistently, bevacizumab treatment can also increase CA-9 expression, and forced downregulation of CA-9 increases responsiveness to bevacizumab (McIntyre et al., 2012). Importantly, the modest change in metabolic gene expression following cediranib treatment was less marked than the difference in expression seen between tumors at baseline. This is illustrated on the PCA plot (Figure S4F).

A recent study demonstrated that switching to a lipogenic phenotype enables tumors to rebound from anti-angiogenic therapy; blocking lipid synthesis via downregulation of *FASN* prevented re-growth (Sounni et al., 2014). To determine whether *FASN* limits cediranib efficacy, mice bearing either NCI-H526 or Calu-6 tumor xenografts were treated with a *FASN* inhibitor (Schug et al., 2015) in combination with cediranib. The anti-tumor effect of cediranib was not significantly improved, suggesting that *FASN* alone is not responsible for the lack of activity in these models (Figure S5A). Together, the published studies and the data outlined here support the concept that both the intrinsic and “on-therapy” metabolic profile of the tumor cell may be important considerations when treating with anti-angiogenics. The data suggest that a “low” glycolytic tumor such as NCI-H526 may undergo a metabolic switch on treatment, whereas the glycolytic VHL null ccRCC A498 model cannot become more glycolytic. Although this concept of metabolic adaption needs further investigation, it provides a plausible link between metabolic phenotype and sensitivity to VEGFi (Sounni et al., 2014).

Leptin Can Modulate the Tumor Metabolic Phenotype

The functional relevance of the metabolic gene expression profiles observed in vivo was explored in vitro. Cell lines from the cediranib-sensitive (CDS) models had a higher glucose consumption rate than insensitive models in vitro, consistent with the glycolytic gene expression signature (Figure 6A). To determine whether leptin influences tumor metabolism, the impact of leptin on glucose utilization in less-sensitive (NCI-H526 and Lovo) and sensitive (SW620) cell lines was analyzed. To mimic the stresses of oxygen and nutrient deficiency caused by cediranib-mediated vessel reduction, cell lines were grown in serum-free media. Leptin caused an increase in glucose consumption by Lovo and NCI-H526 cells, but not by SW620 cells (Figure 6B). Across the panel of cell lines, leptin receptor (*LEPR*) mRNA expression correlated with lactate release (Figure 6C). In the Lovo cell line, glycolytic flux and capacity in response to glucose was increased by leptin, shown by increased extracellular acidification rate (ECAR) without modification of oxygen consumption rate (Figures 6D and S5B). Moreover, leptin-treated Lovo cells were preferentially lost from culture when deprived of glucose, suggesting that leptin increases demand for glucose (Figure S5C).

Leptin-mediated changes in metabolic pathway biomarkers were explored. An increase in PDH phosphorylation occurred in Lovo, but not in NCI-H526, cells (Figure S5D). However, leptin treatment of Lovo cells reduced expression of genes involved in lipid and cholesterol synthesis, including *SREBF2*, *FASN*, *ACACA*, and *NR1H2* in NCI-H526 (Figure 6E). Leptin combined with cediranib treatment also downregulated *FASN* (Figures S5E and S5F). The leptin-induced changes in metabolic gene expression could be attributed to an inhibition of mTOR expression (Figures 6E and 6F). mTOR is involved in the regulation of cell growth, cell proliferation, and metabolism protein synthesis (Morita et al., 2015). The level of pS6, a downstream biomarker of mTOR, was also reduced in NCI-H526 and Lovo, but not in SW620, cells (Figure 6F). Combined leptin and cediranib treatment reduced pS6 staining in Lovo xenografts (Figures 6G and 6H). To model the potential of micro-environmental stress on the tumor cell compartment, cell proliferation of leptin-treated cells in hypoxic and serum-starved conditions was compared. Inhibition of proliferation in NCI-H526 and Lovo cells treated with leptin was seen under hypoxia conditions (Figure S5G). In SW620, leptin had no significant effect on proliferation under any of the conditions explored. It therefore appears that short-term leptin treatment can influence tumor cell metabolic status, stimulating glucose metabolism. In addition, leptin can reduce cell proliferation under conditions of stress such as low oxygen, glucose or serum. The association with changes in the mTOR pathway, in vivo and in vitro, requires further exploration.

Leptin Treatment Does Not Influence the Impact of Cediranib on Endothelial Cells

Leptin receptor (*LEPR*) can be expressed on endothelial cells as well as tumor cells (Bouloumié et al., 1998; Koda et al., 2007b; Wang et al., 2012). Leptin may therefore affect the sensitivity of vessels to cediranib, thereby modulating its efficacy. This was investigated in vitro and in vivo. Leptin did not increase vessel sensitivity to cediranib, as judged by MVD measurements in a tube formation assay in vitro (Figure 7A) or in the Lovo xenograft model (Figures 7B and 7C). This suggests that leptin affects cediranib efficacy primarily via effects on the tumor cell compartment.

Obese Phenotype Increases Cediranib Sensitivity in Mouse Model

To explore whether high leptin associated with obesity affects the efficacy of cediranib, we used the well-characterized Db/Db (obese, high leptin) mouse model. Db/Db and WT (wild-type) control model mice were implanted with B16F10 syngeneic tumors and treated with 3 mg/kg cediranib (Figures 7D and S6). Tumors in both strains responded to cediranib, but cediranib gave greater benefit to tumors in the Db/Db mice (Figure S6A). Although initial tumor growth rate was slower in the Db/Db

(D) Lovo cells were treated with vehicle or leptin 10 ng/ml for 48 hr in serum-free media, and extracellular acidification rate (ECAR) was quantified to assess the glycolytic activity. Error bars represent SD of 3 biological replicates.

(E) Relative gene expression changes observed post-leptin treatment (48 hr) in H526 and Lovo cells lines. Error bars represent SD of 3 biological replicates.

(F) Western blots against mTOR, pS6, S6, and beta-actin on cells treated with leptin.

(G and H) pS6 staining by immunohistochemistry in Lovo xenograft from mice treated with leptin ± cediranib (G) and quantification of the staining (H). Student's t tests were used to determine significance; *p < 0.05.

mice, ulceration with inflammation was more severe and occurred when tumors were smaller. This was accompanied by increased expression of genes involved in matrix remodeling (*mmp2* and *mmp9*) and inflammation (*ccl12*, *ccl2*, *cxcl1*, *cxcl12*, and *il6*) in the tumors of Db/Db mice (Figure S6B). Using the endpoint of tumors either ulcerating or reaching 1 cm³ (Figure S6C), Kaplan-Meier analysis showed that tumors were more sensitive to cediranib in Db/Db compared to WT mice (Figure 7E).

Expression profiling showed that *pdk4*, *hk1*, *pfkfb3*, and *vegfa* were upregulated in tumors from the Db/Db mice (Figure 7F). These genes are also part of the gene signature associated with cediranib sensitivity (Figures 3A and 4A). The expression of genes associated with the cediranib-insensitive signature (CDInS) was not significantly changed in obese compared to non-obese control mice (Figure 7F). Due to high melanin expression in the B16F10 melanoma model, it is challenging to accurately assess MVD by standard immunohistochemical staining of CD31. We therefore analyzed changes in mRNA of the endothelial transcripts *cd31*, *dll4*, *vegfr1*, *vegfr2*, and *vegfr3* to gain insight into changes in vasculature (Farren et al., 2012). Consistent with the observation in Lovo tumors, the tumor vessels in the Db/Db (obese) mice were not more sensitive to cediranib (Figure 7G).

Conclusions

Identifying mechanisms influencing tumor sensitivity to VEGFi is key to effective use of these agents in the clinic. This retrospective analysis of a phase III clinical trial in mCRC comparing chemotherapy versus chemotherapy plus cediranib identified an association of circulating leptin and tumor metabolic status with response to the VEGFi cediranib. It is not clear whether acute signaling or long-term tumor selection pressure are the drivers of the metabolic phenotype. The tumor metabolic profile also associated with response to cediranib in pre-clinical models. These observations reveal a novel link between patient physiology, tumor biology, and clinical response to therapy in mCRC that may apply to other tumor types. To build on these observations, other mCRC clinical samples sets should be interrogated and these biomarkers tested prospectively in a clinic trial.

We suggest that the metabolic status can be listed alongside alternate angiogenic drives (Casanovas et al., 2005), high myeloid-derived cell infiltrate (Shojaei et al., 2007, 2010), and the organization of blood vessels (Bergers et al., 2003; Smith et al., 2013) as a factor that influences tumor response to VEGFi (highlighted in Figure S7). These mechanisms confer tumors with intrinsic resistance or potential to adapt to the reduction in vessels. These additional biomarkers should also be considered to develop an in depth understanding of factors that contribute to VEGFi sensitivity.

EXPERIMENTAL PROCEDURES

HORIZON II Patients

The cohort of patients enrolled in the phase III double-blind HORIZON II study has been detailed previously (Hoff et al., 2012). Because recruitment to the cediranib 30 mg arm was discontinued (Hoff et al., 2012), this study was restricted to patients treated with cediranib 20 mg or placebo in combination with FOLFOX/CAPOX. The HORIZON II clinical trial was performed in accor-

dance with the Declaration of Helsinki, the International Conference on Harmonization/Good Clinical Practice, applicable regulatory requirements, and the AstraZeneca policy on Bioethics.

Serum Protein Analysis

Serum sample collection and quantification of soluble biomarkers was performed as summarized in the Supplemental Experimental Procedures and described previously (Pommier et al., 2014; Spencer et al., 2013). Samples from 582 eligible patients were included as described in the CONSORT diagram (Figure S1).

Gene Expression Analysis from Biopsy Samples

Tumor sample collection was an optional procedure for consenting patients in the HORIZON II study. Investigator sites submitted paraffin-embedded samples from the primary tumor as well as any liver metastases. The samples were handled, formalin fixed, and processed according to local routine practice in clinical pathology. Tissue quality was confirmed by review of an H&E slide by a pathologist. 354 formalin-fixed paraffin-embedded (FFPE) biopsy samples were available in AstraZeneca from this trial. Two sections were cut (Figure S2B), one stained with H&E, and the other retained for RNA extraction. Viable tumor areas were marked on the H&E slide and traced onto the unstained section (Figure S2B). Tumor areas were then macro-dissected for RNA extraction, taking care to exclude normal tissue and areas of necrosis. 95 samples failed QC checks and were excluded (71 for insufficient tumor, 24 for poor RNA quality).

The remaining samples were randomized and total RNA extracted from batches of 24 using the RNeasy FFPE kit from QIAGEN (#73504) following manufacturer's instructions summarized in the Supplemental Experimental Procedures. 100 ng of RNA was used to quantify gene expression using NanoString. Genes associated with leptin, cell metabolism, and angiogenesis were chosen for analysis. Expression was normalized against a pool of housekeeping genes (Table S2).

In Vivo Studies

Tumor xenograft tissue was derived from experiments conducted in accordance with licenses issued under the UK Animals (Scientific Procedures) Act 1986. Cell lines were maintained in the recommended growth medium and implanted subcutaneously into the left flank of 5- to 8-week-old immune-compromised mice (Figure S4G). Mice with established tumors were dosed daily with 3 mg/kg cediranib, 100 mg/kg FASNi (AZ62) (Schug et al., 2015), or vehicle per os (P.O.) as required. For syngeneic experiments, 1 × 10⁵ B16F10 cells were implanted subcutaneously into the left flank of 7-week-old WT or Db/Db mice. Mice were treated daily with 3 mg/kg cediranib or vehicle P.O. Tumors were harvested between 0.8 and 1 cm³ and snap frozen in liquid nitrogen. The mutational status of xenografts was obtained from the Catalogue of Somatic Mutations in Cancer (COSMIC) database based at the Wellcome Trust Sanger Institute.

All animal studies were conducted in accordance with U.K. Home Office legislation, the Animal Scientific Procedures Act 1986, as well as the AstraZeneca Global Bioethics policy. All experimental work is outlined in project license 40/3483, which has gone through the AstraZeneca Ethical Review Process.

Immunohistochemistry

Immunohistochemistry was carried out using routine procedures. The following antibodies were used: CD31 (in-house polyclonal) with Elite ABC (Vector Labs); fatty acid synthase (C20G5) and pS6 (2215S, both Cell Signaling Technology) with anti-rabbit HRP complex (Dako). Counterstained mounted slides were scanned with a ScanScope AT (Aperio), images were quantitated with HALO (Indica Labs) software, and data were processed in Excel (Microsoft) and Spotfire (Tibco).

Cell Culture and Treatment

For the baseline LEPR gene expression analysis, cell lines were grown in phenol-free RPMI 1640 (Sigma), 2 mM glutamine (Gibco), and 10% FCS (SigmaF#7524) in a 5% CO₂ atmosphere at 37°C. When 80% confluent, cells were scraped into 1 ml cold PBS, centrifuged at 1,000 rpm for 2 min, pellets snap frozen, and stored at -80°C. Recombinant human leptin (R&D Systems) at

10 or 100 ng/ml concentration (from 1 mg/ml stock reconstitute in sterile 20 mM Tris-HCL [pH 8.0]) was used. Cells were transferred into FCS-free media 24 hr prior to leptin treatment. NCI-H526, LoVo, and SW620 cells were seeded into 96-well plates at a density of $2.5\text{--}3 \times 10^3$ cells per well and incubated at 37°C, 5% CO₂ at either normoxic (21% oxygen) or hypoxic (0.5% oxygen) conditions. Cells were treated the following day with PBS (vehicle control) or leptin diluted in PBS at 100 ng/ml and 10 ng/ml. Cell numbers were read at 24, 48, and 72 hr for the normoxic plates and at 24 and 48 hr for the hypoxic plates. For each read, cells were incubated in 2 mM Sytox-Green (LifeTech) in TBS + 5 mM EDTA and left for 1 hr at room temperature and read on Acumen at 380V to give the “dead count.” Following this, cells were then incubated in 0.25% Saponin (LifeTech) in TBS + 5 mM EDTA and left for 15 hr at room temperature and read again on the Acumen at 380V to give the “total count.” Live cell number was calculated by taking the total count away from the dead count.

Extracellular Acidification Rate Assay

Cells were plated in a total volume of 80 μ l phenol-free RPMI 1640 (Sigma), 2 mM glutamine (Gibco), and 10% FCS (SigmaF#7524) at 8,000 cell/well density in XF96 PET Cell Culture Microplates (Seahorse Bioscience, #101104-004) and left to adhere overnight at 37°C, 5% CO₂. The next day, cells were transferred in a FCS-free media. After 24 hr, cells were treated with 10 ng/ml leptin in FCS-free RPMI 1640 for 48 hr. The medium was then replaced with 180 μ l unbuffered, glucose-free DMEM XF assay medium (Seahorse Bioscience, #100965-000) containing 2 mM glutamine (Gibco), 1% penicillin/streptavidin (Invitrogen), and the appropriate concentration of leptin. The pH was adjusted to 7.41 using 1N sodium hydroxide, and the medium was filter-sterilized through a 0.2 μ m pore size filter (Fischer Scientific, #TKV260030S). ECAR measurement was performed as recommended by the manufacturer and described in the [Supplemental Experimental Procedures](#).

Measuring Glucose Levels in the Media

Glucose levels were measured at room temperature using the Accu-Chek Mobile System (Roche) according to manufacturer's protocol. Cells were seeded in duplicate in triplicate experiments (4×10^3 cells per well, 100 μ l) into Costar clear flat bottom 96-well plates. Cell medium was changed 24 hr after seeding to DMEM (#D5921) (Sigma) supplemented with 10 mM D-glucose (Sigma), 2 mM L-glutamine (Sigma), and 10% dialysed fetal bovine serum (FBS) (Thermo Scientific). Following a second medium change, cells were treated with leptin diluted in phosphate-buffered saline (PBS) or PBS alone as a control. Medium samples were taken at 0, 1, 6, 24, and 48 hr post-treatment, and glucose levels were normalized to the initial cell number made on a parallel 96-well plate, read at 0 hr.

Tube Formation Assay

Normal human dermal fibroblasts (NHDFs) (Promocell) were seeded at 2,000 cells per well in 96-well collagen-coated plates in fibroblast growth media (Promocell) (100 μ l per well) and incubated at 37°C, 5% CO₂ for 72 hr. The media was aspirated and HUVECs (Promocell) seeded onto the NHDF monolayer at 5,400 cells per well in 100 μ l of MCDB131, 10% FCS, 2 mM L-glutamine and incubated overnight at 37°C, 5% CO₂. The following day, day 1 of the assay, the co-cultures were treated with VEGF, leptin, and cediranib titrations as indicated in growth media supplemented with 2% FBS. Media was aspirated and the tube plates redosed on days 4 and 8 and the assay finished and the cells fixed with 100% ethanol on day 11. The cells were washed once with PBS and blocked for 1 hr at 37°C in PBS, 1% BSA. The block was removed and the cells stained with mouse anti-human CD31-Alexa 488 (BD Biosciences) (1:500 dilution) and Hoechst 33342 (1 in 5,000 dilution) in PBS, 1% BSA. The cells were washed 2 \times with PBS and 100 μ l of PBS added to the well. The fluorescence was imaged on the Cellomics Arrayscan and tube formation quantitated.

Gene Expression Profiling from Xenografts and Cell Lines

1×10^6 cells or 50 mg of tissue were cut from the frozen tumors, and RNA was isolated by using the RNeasy MiniKit (QIAGEN), following the manufacturer's protocol. On-column DNase digestion was performed using the RNase-free DNase Kit (QIAGEN). RNA concentration was measured using the NanoDrop ND1000 (NanoDrop); RNA integrity (RIN) was assessed using

the RNA 6000 Nano Assay (Agilent Technologies); RIN values for all samples were between 7 and 10. Human-specific assays were designed and supplied by Applied Biosystems. Eukaryotic 18S rRNA was used as the endogenous control. Reverse transcription and preamplification were performed as recommended by Applied Biosystems and further described in the [Supplemental Experimental Procedures](#). Samples were diluted 1 in 5 with TE and stored at -20°C . Sample and assay preparation for 48.48 Fluidigm Dynamic arrays was done according to the manufacturer's instructions. Briefly, samples were mixed with 20 \times sample loading reagent (Fluidigm) and TaqMan Gene Expression Master Mix (Applied Biosystems). Assays were mixed with 2 \times assay loading reagent (Fluidigm). The 48.48 Fluidigm Dynamic Arrays (Fluidigm) were primed and loaded on an IFC Controller (Fluidigm), and qPCR experiments were run on a Biomark System (Fluidigm) using the following thermal profile: 50°C for 2 min, 95°C for 10 min, and 40 cycles of 95°C for 15 s and 60°C for 1 min. Data were collected and analyzed using the Fluidigm Real-Time PCR Analysis 2.1.1 software. Gene expression values were calculated using the comparative CT ($-\Delta\text{CT}$) method as previously described in User Bulletin #2 ABI PRISM 7700 Sequence Detection System 10/2001, using the corrected 18S rRNA CT value to determine changes in the context of the entire mRNA pool.

Metabolomic Analyses

Metabolites were extracted from frozen tissue. Chromatographic analysis was performed on an Ultimate 3000 RS pump combined with an Ultimate 3000 autosampler operating at 4°C through Chromeleon software package (Thermo). Mass spectrometry was performed on a 4000 QTRAP hybrid triple quadrupole linear ion trap mass spectrometer operating through Analyst 1.5.1 (Applied Biosystems/MDS Sciex). Further information is provided in the [Supplemental Experimental Procedures](#).

Western Blot

Proteins were extracted using 100 μ l cell lysis buffer composed of: 25 mM Tris/HCl (Sigma #T-1535), 3 mM EDTA (Sigma #E-7889), 3 mM EGTA (Sigma #E-0396), 50 mM NaF (Sigma #S-1504), 2 mM orthovanadate (Sigma #S-6508), 0.27 M sucrose (Fisher #S/8600/60), 10 mM β -glycerophosphate (Sigma #G-6251), 5 mM Na-pyrophosphate (Sigma #S-6422), 0.5% Triton X-100 (Sigma #T-9284) supplemented with fresh complete protease inhibitor (Roche #11-836-153-001) and phosphatase inhibitor cocktail 3 (Sigma #-P0044). Proteins of interest were detected with the following antibodies: Anti-PDH-E1a (pSer²⁹³) (Millipore #AP1062), Anti-PDH (CST #2784), Anti-mTOR (CST #2972), Anti- β -Actin (Sigma #A2228), Anti-Phospho-S6 Ribosomal Protein (Ser235/236) (2F9) (CST #4856), and Anti-S6 Ribosomal Protein (CST #4856).

Statistical Methods

Clinical Analyses

The association with clinical end points was estimated using a Cox regression model performed in R 2.13 for the large-scale analyses ([Figures 1, 3, and S3](#)). To verify the predictive values for BMI, leptin, and gene signatures on PFs and OS, we used a Kaplan-Meier method and Cox model in SigmaPlot 11. Hierarchical clusters, heatmaps, volcano plots, and forest plots were created using TIBCO Spotfire. The primary covariates used in the trial were World Health Organization (WHO) performance status, chemotherapy received, baseline liver function, and study phase; these were balanced between treatment arms. Due to the reduced sample size, we chose to omit the primary covariates from the analyses. A comparison of the full HORIZON II analysis with and without the covariates showed very comparable HRs and CIs ([Spencer et al., 2013](#)).

Regarding the statistical analyses aiming to assess the impact of the 207 serum protein concentrations on clinical outcome in patients treated with chemotherapy \pm cediranib, we used a methodology different from that described by [Spencer et al. \(2013\)](#). In [Spencer et al. \(2013\)](#), the predictive analysis on OS and PFS was performed by comparison of chemotherapy plus placebo versus chemotherapy plus cediranib using two Cox regression models: (1) in patients defined as a low group and (2) in patients defined as high group (relative to median). Here, we have compared the impact of biomarker concentrations (high versus low groups, still relative to median) using two Cox regression models: (1) in patients treated with chemotherapy plus

placebo and (2) in patients treated with chemotherapy plus cediranib. $p < 0.05$ was considered significant.

To examine the association between tumor gene expression and clinical outcomes, we used statistical approaches. First we dichotomized patients into high and low groups (relative to median expression) and compared the PFS and OS in patients treated with chemotherapy plus placebo versus chemotherapy plus cediranib using a Cox model (R 2.13). Genes found significantly correlated with outcomes ($p < 0.05$) were then classified into two categories according to whether they were associated with improved outcome in response to cediranib in high or low group. Within each category, genes were classified according to the p value of the HR obtained by the Cox regression model. To obtain co-expressed gene clusters and patient stratification, hierarchical clustering analysis was used with the following parameters: Ward's clustering method, half-square Euclidean for the distance measure, average value for the ordering weight, and Z score calculation for the normalization.

The correlation between BMI and leptin concentrations was assessed using linear regression analysis with TIBCO Spotfire.

Mann-Whitney test was used to examine the significance of the correlations observed between gene expression and serum leptin concentrations.

Pre-clinical Analyses

Gene expression values were calculated using the comparative Ct ($-DCt$) method as previously described in User Bulletin #2 ABI PRISM 7700 Sequence Detection System 10/2001, using the human 18S rRNA Ct values for normalization. Validation experiments of this platform indicated the confidence limit of detection of this technology was a Ct of 35. Therefore, missing data and Ct values of 35 were imputed with a Ct value of 35. This ensured that correlation analysis incorporated the low expression data rather than excluding it. Linear regression was performed using TIBCO Spotfire, with p values < 0.05 considered as significant. Relative expression changes were calculated using DDCT method. In Figure 5A, highly sensitive or less-sensitive groups were defined based on the average of the sensitivity (76.7% tumor growth inhibition) across the 13 models.

For the mass spectrometry analyses, coefficients of variation (CVs, $SD/\text{mean} \times 100$) were calculated for each QC analyte. Modulated metabolites met all of the following criteria: (a) QC CV < 30 , (b) p value < 0.05 and absolute \log_2 fold change > 0.05 . Unless indicated otherwise, t tests were used to determine significance.

SUPPLEMENTAL INFORMATION

Supplemental Information includes Supplemental Experimental Procedures, seven figures, and three tables and can be found with this article online at <http://dx.doi.org/10.1016/j.cmet.2015.10.015>.

CONFLICT OF INTEREST

A.J.C.P., M.F., B.P., M.W., H.C., C.W., F.M., N.R.S., J.K., J.F., R.H., C.E., P.D.S., J.R., S.M., S.E.C., and S.T.B. are current or former employees of AstraZeneca. N.R.S., J.K., J.F., C.E., P.D.S., J.R., H.C., S.M., S.E.C., and S.T.B. are shareholders in AstraZeneca.

ACKNOWLEDGMENTS

Funding for this study was provided by AstraZeneca. A.J.C.P. was a postdoc Marie Curie Fellow in the EU FP7-funded Initial Training Network TransVIR from 2011 to 2013 and funded by AstraZeneca from 2013. We would like to thank Dr. Juliane Jürgensmeier for her comments during the early steps of this work.

Received: August 14, 2014

Revised: July 30, 2015

Accepted: October 26, 2015

Published: November 25, 2015

REFERENCES

Bergers, G., and Hanahan, D. (2008). Modes of resistance to anti-angiogenic therapy. *Nat. Rev. Cancer* 8, 592–603.

Bergers, G., Song, S., Meyer-Morse, N., Bergsland, E., and Hanahan, D. (2003). Benefits of targeting both pericytes and endothelial cells in the tumor vasculature with kinase inhibitors. *J. Clin. Invest.* 111, 1287–1295.

Bokacheva, L., Kotedia, K., Reese, M., Ricketts, S.A., Halliday, J., Le, C.H., Koutcher, J.A., and Carlin, S. (2013). Response of HT29 colorectal xenograft model to cediranib assessed with 18 F-fluoromisonidazole positron emission tomography, dynamic contrast-enhanced and diffusion-weighted MRI. *NMR Biomed.* 26, 151–163.

Bouloumié, A., Drexler, H.C., Lafontan, M., and Busse, R. (1998). Leptin, the product of Ob gene, promotes angiogenesis. *Circ. Res.* 83, 1059–1066.

Brauer, M.J., Zhuang, G., Schmidt, M., Yao, J., Wu, X., Kaminker, J.S., Jurinka, S.S., Kolumam, G., Chung, A.S., Jubb, A., et al. (2013). Identification and analysis of in vivo VEGF downstream markers link VEGF pathway activity with efficacy of anti-VEGF therapies. *Clin. Cancer Res.* 19, 3681–3692.

Brave, S.R., Ratcliffe, K., Wilson, Z., James, N.H., Ashton, S., Wainwright, A., Kendrew, J., Dudley, P., Broadbent, N., Sproat, G., et al. (2011). Assessing the activity of cediranib, a VEGFR-2/3 tyrosine kinase inhibitor, against VEGFR-1 and members of the structurally related PDGFR family. *Mol. Cancer Ther.* 10, 861–873.

Casanovas, O., Hicklin, D.J., Bergers, G., and Hanahan, D. (2005). Drug resistance by evasion of antiangiogenic targeting of VEGF signaling in late-stage pancreatic islet tumors. *Cancer Cell* 8, 299–309.

Chung, A.S., Wu, X., Zhuang, G., Ngu, H., Kasman, I., Zhang, J., Vernes, J.M., Jiang, Z., Meng, Y.G., Peale, F.V., et al. (2013). An interleukin-17-mediated paracrine network promotes tumor resistance to anti-angiogenic therapy. *Nat. Med.* 19, 1114–1123.

Crawford, Y., Kasman, I., Yu, L., Zhong, C., Wu, X., Modrusan, Z., Kaminker, J., and Ferrara, N. (2009). PDGF-C mediates the angiogenic and tumorigenic properties of fibroblasts associated with tumors refractory to anti-VEGF treatment. *Cancer Cell* 15, 21–34.

di Tomaso, E., Snuderl, M., Kamoun, W.S., Duda, D.G., Auluck, P.K., Fazlollahi, L., Andronesi, O.C., Frosch, M.P., Wen, P.Y., Plotkin, S.R., et al. (2011). Glioblastoma recurrence after cediranib therapy in patients: lack of “rebound” revascularization as mode of escape. *Cancer Res.* 71, 19–28.

Ebos, J.M., Lee, C.R., and Kerbel, R.S. (2009). Tumor and host-mediated pathways of resistance and disease progression in response to antiangiogenic therapy. *Clin. Cancer Res.* 15, 5020–5025.

Ellis, L.M., and Hicklin, D.J. (2008). VEGF-targeted therapy: mechanisms of anti-tumour activity. *Nat. Rev. Cancer* 8, 579–591.

Farren, M., Weston, S., Brown, H., Broadbent, N., Powell, S., Shaw, R., Smith, N.R., Inglis, R., Graham, A., Ashton, S., et al. (2012). Expression of stromal genes associated with the angiogenic response are not differentiated between human tumour xenografts with divergent vascular morphologies. *Angiogenesis* 15, 555–568.

Garofalo, C., and Surmacz, E. (2006). Leptin and cancer. *J. Cell. Physiol.* 207, 12–22.

Guiu, B., Petit, J.M., Bonnetain, F., Ladoire, S., Guiu, S., Cercueil, J.P., Krausé, D., Hillon, P., Borg, C., Chauffert, B., and Ghiringhelli, F. (2010). Visceral fat area is an independent predictive biomarker of outcome after first-line bevacizumab-based treatment in metastatic colorectal cancer. *Gut* 59, 341–347.

Hanahan, D., and Weinberg, R.A. (2011). Hallmarks of cancer: the next generation. *Cell* 144, 646–674.

Helfrich, I., Scheffrahn, I., Bartling, S., Weis, J., von Felbert, V., Middleton, M., Kato, M., Ergün, S., Augustin, H.G., and Schadendorf, D. (2010). Resistance to antiangiogenic therapy is directed by vascular phenotype, vessel stabilization, and maturation in malignant melanoma. *J. Exp. Med.* 207, 491–503.

Hoff, P.M., Hochhaus, A., Pestalozzi, B.C., Tebbutt, N.C., Li, J., Kim, T.W., Koynov, K.D., Kurteva, G., Pintér, T., Cheng, Y., et al. (2012). Cediranib plus FOLFOX/CAPOX versus placebo plus FOLFOX/CAPOX in patients with previously untreated metastatic colorectal cancer: a randomized, double-blind, phase III study (HORIZON II). *J. Clin. Oncol.* 30, 3596–3603.

Hurwitz, H., Fehrenbacher, L., Novotny, W., Cartwright, T., Hainsworth, J., Heim, W., Berlin, J., Baron, A., Griffing, S., Holmgren, E., et al. (2004).

- Bevacizumab plus irinotecan, fluorouracil, and leucovorin for metastatic colorectal cancer. *N. Engl. J. Med.* **350**, 2335–2342.
- Jain, R.K., Duda, D.G., Clark, J.W., and Loeffler, J.S. (2006). Lessons from phase III clinical trials on anti-VEGF therapy for cancer. *Nat. Clin. Pract. Oncol.* **3**, 24–40.
- Jain, M., Nilsson, R., Sharma, S., Madhusudhan, N., Kitami, T., Souza, A.L., Kafri, R., Kirschner, M.W., Clish, C.B., and Mootha, V.K. (2012). Metabolite profiling identifies a key role for glycine in rapid cancer cell proliferation. *Science* **336**, 1040–1044.
- Koda, M., Sulkowska, M., Kanczuga-Koda, L., Cascio, S., Colucci, G., Russo, A., Surmacz, E., and Sulkowski, S. (2007a). Expression of the obesity hormone leptin and its receptor correlates with hypoxia-inducible factor-1 alpha in human colorectal cancer. *Ann. Oncol.* **18** (Suppl 6), vi116–vi119.
- Koda, M., Sulkowska, M., Kanczuga-Koda, L., Surmacz, E., and Sulkowski, S. (2007b). Overexpression of the obesity hormone leptin in human colorectal cancer. *J. Clin. Pathol.* **60**, 902–906.
- Koukourakis, M.I., Giatromanolaki, A., Sivridis, E., Gatter, K.C., Trarbach, T., Folprecht, G., Shi, M.M., Leibold, D., Jalava, T., Laurent, D., et al. (2011). Prognostic and predictive role of lactate dehydrogenase 5 expression in colorectal cancer patients treated with PTK787/ZK 222584 (vatalanib) antiangiogenic therapy. *Clin. Cancer Res.* **17**, 4892–4900.
- Larsson, S.C., and Wolk, A. (2007). Obesity and colon and rectal cancer risk: a meta-analysis of prospective studies. *Am. J. Clin. Nutr.* **86**, 556–565.
- Li, J.L., Sainson, R.C., Oon, C.E., Turley, H., Leek, R., Sheldon, H., Bridges, E., Shi, W., Snell, C., Bowden, E.T., et al. (2011). DLL4-Notch signaling mediates tumor resistance to anti-VEGF therapy in vivo. *Cancer Res.* **71**, 6073–6083.
- Locasale, J.W., Grassian, A.R., Melman, T., Lyssiotis, C.A., Mattaini, K.R., Bass, A.J., Heffron, G., Metallo, C.M., Muranen, T., Sharfi, H., et al. (2011). Phosphoglycerate dehydrogenase diverts glycolytic flux and contributes to oncogenesis. *Nat. Genet.* **43**, 869–874.
- Lu, D., Jimenez, X., Zhang, H., Bohlen, P., Witte, L., and Zhu, Z. (2002). Selection of high affinity human neutralizing antibodies to VEGFR2 from a large antibody phage display library for antiangiogenesis therapy. *Int. J. Cancer* **97**, 393–399.
- Ma, Y., Yang, Y., Wang, F., Zhang, P., Shi, C., Zou, Y., and Qin, H. (2013). Obesity and risk of colorectal cancer: a systematic review of prospective studies. *PLoS ONE* **8**, e53916.
- McIntyre, A., Patiar, S., Wigfield, S., Li, J.L., Ledaki, I., Turley, H., Leek, R., Snell, C., Gatter, K., Sly, W.S., et al. (2012). Carbonic anhydrase IX promotes tumor growth and necrosis in vivo and inhibition enhances anti-VEGF therapy. *Clin. Cancer Res.* **18**, 3100–3111.
- Morita, M., Gravel, S.P., Hulea, L., Larsson, O., Pollak, M., St-Pierre, J., and Topisirovic, I. (2015). mTOR coordinates protein synthesis, mitochondrial activity and proliferation. *Cell Cycle* **14**, 473–480.
- Nardo, G., Favaro, E., Curtarello, M., Moserle, L., Zulato, E., Persano, L., Rossi, E., Esposito, G., Crescenzi, M., Casanovas, O., et al. (2011). Glycolytic phenotype and AMP kinase modify the pathologic response of tumor xenografts to VEGF neutralization. *Cancer Res.* **71**, 4214–4225.
- Park, H.Y., Kwon, H.M., Lim, H.J., Hong, B.K., Lee, J.Y., Park, B.E., Jang, Y., Cho, S.Y., and Kim, H.S. (2001). Potential role of leptin in angiogenesis: leptin induces endothelial cell proliferation and expression of matrix metalloproteinases in vivo and in vitro. *Exp. Mol. Med.* **33**, 95–102.
- Park, J., Kusminski, C.M., Chua, S.C., and Scherer, P.E. (2010). Leptin receptor signaling supports cancer cell metabolism through suppression of mitochondrial respiration in vivo. *Am. J. Pathol.* **177**, 3133–3144.
- Pommier, A.J., Shaw, R., Spencer, S.K., Morgan, S.R., Hoff, P.M., Robertson, J.D., Barry, S.T., and Jürgensmeier, J.M. (2014). Serum protein profiling reveals baseline and pharmacodynamic biomarker signatures associated with clinical outcome in mCRC patients treated with chemotherapy ± cediranib. *Br. J. Cancer* **111**, 1590–1604.
- Possemato, R., Marks, K.M., Shaul, Y.D., Pacold, M.E., Kim, D., Birsoy, K., Sethumadhavan, S., Woo, H.K., Jang, H.G., Jha, A.K., et al. (2011). Functional genomics reveal that the serine synthesis pathway is essential in breast cancer. *Nature* **476**, 346–350.
- Schug, Z.T., Peck, B., Jones, D.T., Zhang, Q., Grosskurth, S., Alam, I.S., Goodwin, L.M., Smethurst, E., Mason, S., Blyth, K., et al. (2015). Acetyl-CoA synthetase 2 promotes acetate utilization and maintains cancer cell growth under metabolic stress. *Cancer Cell* **27**, 57–71.
- Shojaei, F., and Ferrara, N. (2008). Refractoriness to antivascular endothelial growth factor treatment: role of myeloid cells. *Cancer Res.* **68**, 5501–5504.
- Shojaei, F., Wu, X., Malik, A.K., Zhong, C., Baldwin, M.E., Schanz, S., Fuh, G., Gerber, H.P., and Ferrara, N. (2007). Tumor refractoriness to anti-VEGF treatment is mediated by CD11b+Gr1+ myeloid cells. *Nat. Biotechnol.* **25**, 911–920.
- Shojaei, F., Lee, J.H., Simmons, B.H., Wong, A., Esparza, C.O., Plumlee, P.A., Feng, J., Stewart, A.E., Hu-Lowe, D.D., and Christensen, J.G. (2010). HGF/c-Met acts as an alternative angiogenic pathway in sunitinib-resistant tumors. *Cancer Res.* **70**, 10090–10100.
- Simkens, L.H., Koopman, M., Mol, L., Veldhuis, G.J., Ten Bokkel Huinink, D., Muller, E.W., Derleyn, V.A., Teerenstra, S., and Punt, C.J. (2011). Influence of body mass index on outcome in advanced colorectal cancer patients receiving chemotherapy with or without targeted therapy. *Eur. J. Cancer* **47**, 2560–2567.
- Smith, N.R., Baker, D., Farren, M., Pommier, A., Swann, R., Wang, X., Mistry, S., McDaid, K., Kendrew, J., Womack, C., et al. (2013). Tumor stromal architecture can define the intrinsic tumor response to VEGF-targeted therapy. *Clin. Cancer Res.* **19**, 6943–6956.
- Sounni, N.E., Cimino, J., Blacher, S., Primac, I., Truong, A., Mazzucchelli, G., Paye, A., Calligaris, D., Debois, D., De Tullio, P., et al. (2014). Blocking lipid synthesis overcomes tumor regrowth and metastasis after antiangiogenic therapy withdrawal. *Cell Metab.* **20**, 280–294.
- Spencer, S.K., Pommier, A.J., Morgan, S.R., Barry, S.T., Robertson, J.D., Hoff, P.M., and Jürgensmeier, J.M. (2013). Prognostic/predictive value of 207 serum factors in colorectal cancer treated with cediranib and/or chemotherapy. *Br. J. Cancer* **109**, 2765–2773.
- Steffens, S., Grünwald, V., Ringe, K.I., Seidel, C., Eggers, H., Schrader, M., Wacker, F., Kuczyk, M.A., and Schrader, A.J. (2011). Does obesity influence the prognosis of metastatic renal cell carcinoma in patients treated with vascular endothelial growth factor-targeted therapy? *Oncologist* **16**, 1565–1571.
- Swinnen, J.V., Roskams, T., Joniau, S., Van Poppel, H., Oyen, R., Baert, L., Hejns, W., and Verhoeven, G. (2002). Overexpression of fatty acid synthase is an early and common event in the development of prostate cancer. *Int. J. Cancer* **98**, 19–22.
- Tran, H.T., Liu, Y., Zurita, A.J., Lin, Y., Baker-Neblett, K.L., Martin, A.M., Figlin, R.A., Hutson, T.E., Sternberg, C.N., Amado, R.G., et al. (2012). Prognostic or predictive plasma cytokines and angiogenic factors for patients treated with pazopanib for metastatic renal-cell cancer: a retrospective analysis of phase 2 and phase 3 trials. *Lancet Oncol.* **13**, 827–837.
- Vander Heiden, M.G., Lunt, S.Y., Dayton, T.L., Fiske, B.P., Israelsen, W.J., Mattaini, K.R., Vokes, N.I., Stephanopoulos, G., Cantley, L.C., Metallo, C.M., and Locasale, J.W. (2011). Metabolic pathway alterations that support cell proliferation. *Cold Spring Harb. Symp. Quant. Biol.* **76**, 325–334.
- Vucenik, I., and Stains, J.P. (2012). Obesity and cancer risk: evidence, mechanisms, and recommendations. *Ann. N Y Acad. Sci.* **1271**, 37–43.
- Wang, D., Chen, J., Chen, H., Duan, Z., Xu, Q., Wei, M., Wang, L., and Zhong, M. (2012). Leptin regulates proliferation and apoptosis of colorectal carcinoma through PI3K/Akt/mTOR signalling pathway. *J. Biosci.* **37**, 91–101.
- Wedge, S.R., Kendrew, J., Hennequin, L.F., Valentine, P.J., Barry, S.T., Brave, S.R., Smith, N.R., James, N.H., Dukes, M., Curwen, J.O., et al. (2005). AZD2171: a highly potent, orally bioavailable, vascular endothelial growth factor receptor-2 tyrosine kinase inhibitor for the treatment of cancer. *Cancer Res.* **65**, 4389–4400.
- Widjaja, A., Stratton, I.M., Horn, R., Holman, R.R., Turner, R., and Brabant, G. (1997). UKPDS 20: plasma leptin, obesity, and plasma insulin in type 2 diabetic subjects. *J. Clin. Endocrinol. Metab.* **82**, 654–657.

- Wilson, P.M., Yang, D., Azuma, M., Shi, M.M., Danenberg, K.D., Lebwohl, D., Sherrad, A., Ladner, R.D., Zhang, W., Danenberg, P.V., et al. (2013). Intratumoral expression profiling of genes involved in angiogenesis in colorectal cancer patients treated with chemotherapy plus the VEGFR inhibitor PTK787/ZK 222584 (vatalanib). *Pharmacogenomics J.* 13, 410–416.
- Xu, L., Duda, D.G., di Tomaso, E., Ancukiewicz, M., Chung, D.C., Lauwers, G.Y., Samuel, R., Shellito, P., Czitko, B.G., Lin, P.C., et al. (2009). Direct evidence that bevacizumab, an anti-VEGF antibody, up-regulates SDF1alpha, CXCR4, CXCL6, and neuropilin 1 in tumors from patients with rectal cancer. *Cancer Res.* 69, 7905–7910.
- Yehuda-Shnaidman, E., Nimri, L., Tarnovskii, T., Kirshtein, B., Rudich, A., and Schwartz, B. (2013). Secreted human adipose leptin decreases mitochondrial respiration in HCT116 colon cancer cells. *PLoS ONE* 8, e74843.
- Zheng, J. (2012). Energy metabolism of cancer: Glycolysis versus oxidative phosphorylation (Review). *Oncol. Lett.* 4, 1151–1157.

Cell Metabolism, Volume 23

Supplemental Information

Leptin, BMI, and a Metabolic Gene Expression Signature Associated with Clinical Outcome to VEGF Inhibition in Colorectal Cancer

Aurélien J.C. Pommier, Matthew Farren, Bhavika Patel, Mark Wappett, Filippos Michopoulos, Neil R. Smith, Jane Kendrew, Jeremy Frith, Russell Huby, Catherine Eberlein, Hayley Campbell, Christopher Womack, Paul D. Smith, Jane Robertson, Shethah Morgan, Susan E. Critchlow, and Simon T. Barry

Supplemental experimental procedures

Serum protein analysis

Collection of blood samples from consenting patients was prescribed (but not monitored) as follow: sampling into serum separated tubes and centrifuged within 1 hour for 15 minutes at 3000g, aliquoted into vials and stored immediately at -80°C . Frozen serum samples were shipped and analyzed centrally at Rules-Based Medicine (Myriad RBM, Austin, TX). Analyzed proteins were selected based on their relevance to angiogenesis and linked to tumor progression. Additional analytes were included if they were multiplexed with the requested markers. Each aliquot was thawed to measure 207 proteins that were quantified by using a Luminex bead-based multiplex immunodetection methodology. Myriad RBM's multi-analyte profiles (MAPs) have been validated to Clinical Laboratory Standards Institute (formerly NCCLS) guidelines based upon the principles of immunoassay. Each assay is developed as a single test to establish the sensitivity and dynamic range necessary for that analyte. Key performance parameters such as lower limit of quantification, precision, cross-reactivity, linearity, spike-recovery, dynamic range, matrix interference, freeze-thaw stability, and short-term sample stability are established for every assay (<http://www.myriadrbm.com/>).

RNA extraction from biopsy samples, quantification and quality control

Total RNA was extracted from FFPE samples using RNeasy FFPE kit from Qiagen (cat. number #73504) following manufacturer's instructions. Briefly, using a scalpel, one 5uM tumor section was scraped from a slide into a microcentrifuge tube containing deparaffinization solution from Qiagen (#19093). Samples were vortexed for 10s, centrifuged and incubated at 56°C with proteinase K overnight. The next day, samples were incubated with DNase I for 15 min and RNA was purified using Qiagen columns as described in the kit's instructions in 28uL elution volume.

RNA was quantified by NanoDrop and samples with a yield < 5 ng/μL and/or a 260/280 ratio < 1.6 were not included in any further analysis.

Glucose dependency assay

All cell lines were cultured RPMI 1640 (Sigma), 2 mM glutamine (GIBCO) and 10% FCS (SigmaF#7524). Assay media was composed of phenol red-free, glucose-free DMEM (Sigma), 1% Pen-strep (GIBCO) and 10% sterile filtered dialyzed fetal calf serum (GIBCO). Cells were incubated at 37°C/5% CO₂ during the whole assay. Cells were seeded in 384 well plates accordingly to allow 90% confluence after 7 days growth in assay media supplemented with 25 mM glucose (Sigma) and 2 mM L-glutamine (GIBCO). Cultures were seeded in assay media and incubated overnight to allow adherence. Cells were dosed the following day with appropriate doses of glucose. The assay plates were stained after 7 days for 1 hour at room temperature and pressure (rtp) with 2 mM Sytox Green in TBS + 5mM EDTA and a “dead” cell count was measured using the Acumen reader at 390V. Immediately following the “dead” read the cells were incubated with 0.25% Saponin in TBS + 5 mM EDTA for 16 hours at rtp and read again on the Acumen reader to give a “total” cell count. The “total” cell count was then subtracted from the dead cell count to give a “live” cell number. The live cell count was normalized against growth in 25 mM glucose and 2 mM glutamine to give a relative % growth.

Extracellular acidification rate assay

The plate was transferred into a 37 °C, CO₂ free incubator for 2 hours prior to XF96 assay start. Before XF96 assay starts, the disposable sensor cartridges were hydrated in 200 μl Seahorse Calibrant fluid (Seahorse Bioscience, #100840-000), as advised by the manufacturer overnight and various compounds (20 μl Glucose for 11 mM final concentration), 22 μl of Oligomycin A, (Sigma, # 75351 for 1μM final concentration) and 24 μl of 2-Deoxy-Glucose (20mM final concentration) injection were added to either port A, B or C of the cartridge. ECAR measured at baseline and monitored over time using XF96 Seahorse Analyzer Data Analysis Program. This

calculated averages, standard deviation, % increases / decreases over baseline measurements and accounted for background readings in media-only control wells.

Reverse transcription and pre-amplification of RNA from xenografts and cell lines

5 ng of RNA was used in the reverse transcription using the High Capacity cDNA Reverse transcription kit (Applied Biosystems) in final volume of 20 μ l. The following thermal profile was used: 25°C for 10 minutes, 37°C for 120 minutes, 85°C for 5 second and 4°C for 2 minutes in a total volume of 20 μ l. 1.25 μ l were pre-amplified using a pool of TaqMan primers at a final dilution of 1 in 100 and pre-amplification master Mix (Applied Biosystems) in a final volume of 5 μ l. The following thermal profile was used; 95°C for 10 minutes, 14 cycles of 95°C for 15 seconds and 60°C for 4 minutes.

Metabolomic analyses

Frozen tissue was homogenized and extracted using a 2 ml CK14 Precellys kit. 1ml ACN/MeOH/H₂O 40/40/20 (-20C) per 100mg of tissue was added to the lysing tube and samples followed to cycle of 20sec shake each at 6500rpm with the interim pause of 20 seconds. Precellys chamber temperature was kept at 8-9°C throughout the extraction. Clear supernatant was obtained after centrifugation at 20900g at 4°C for 5min and aliquoted to cryogenic vials to store at -20C. Prior to sample analysis 25 μ l of each sample was placed on a polypropylene HPLC vial and reduce to dryness using under vaccum conditions in a Savant SPD2010 SpeedVac (Thermo Fisher) for approximately 1 hour. Dry residual was resuspended at 50ml of ultrapure water and centrifuged at 3270 g for 10 min at 4°C (Allegra X12R equipped with SX4750A swinging bucket rotor Beckam Coulter). To monitor analytical variability a pooled sample (QC) was generated by mixing equal aliquotes of each individual tissue extracts and treated another sample through the sample preparation procedure.

Chromatographic analysis was performed on an Ultimate 3000 RS pump combined with an Ultimate 3000 autosampler operating at 4°C through Chromeleon software package (Thermo).

Separations were performed on an Acquity HSS T3 UPLC column (2.1×100 mm, 1.8 μm particle size, Waters). Column temperature was maintained at 60±0.5°C during the analysis. 5 μl of samples were injected and elution was performed using a binary solvent system consisting of solvent A (H₂O, 15mM TBA, 10mM Acetic Acid) and solvent B (80% MeOH and 20% isopropanol). The optimum chromatographic separation was achieved with a flow rate of 400 μl/min and the following gradient elution profile: 0 min, 0% B; 0.5 min, 0% B; 4 min, 5% B; 6 min, 5% B; 6.5 min, 20% B; 8.5 min, 20% B; 14 min, 55% B; 15 min, 100% B; 17 min, 100% B; 18 min, 0% B; 21 min 0% B. Samples were analysed in random order with QC sample been analysed in regular intervals to access system performance and variability.

All of the MS data was acquired on a 4000 QTRAP hybrid triple quadrupole linear ion trap mass spectrometer operating through Analyst 1.5.1 (Applied Biosystems/MDS Sciex, Warrington, U.K.). The TurboIonSpray voltage was set at -3500 V, curtain gas at 10, temperature to 550°C, Gas1 and 2 were set at 60 and 50 respectively and entrance potential at -10V. Data was acquired in negative mode using the scheduled MRM transitions shown in Table S1. To obtain the optimum MS parameters each individual standard was dissolved in MeOH/H₂O 50/50 at concentration of 10μM and infused at 10μL/min flow. Peak integration was performed using the MultiQuant software. All sample peaks were compared to the standards and standards+QC mix to ensure that the correct peak was selected. Normalisation to median sample metabolic profile was applied.

Supplemental legends

Figure S1 (Related to Figure 2)

A. Kaplan-Meier analyses showing the impact of high versus low leptin serum concentrations and PFS in response to chemotherapy \pm cediranib. **B.** Kaplan-Meier curves showing the impact of high versus low BMI on PFS in response to chemotherapy \pm cediranib.

PFS: Progression Free Survival; HR: Hazard Ratio; CI: Confident Interval; BMI: Body Mass Index.

Figure S2 (Related to Figure 3)

A. CONSORT diagram of the tumor biopsies used for gene expression profiling in HORIZON II trial. **B.** Schematic view of the methodology used to identify genes associated with clinical outcomes in HORIZON II trial. **C.** The forest plot represents the impact of treatment (chemo-plac vs chemo-ced) in patient groups defined as high and low expression (relative to the median for each gene) on PFS for the significant genes ($P < 0.05$). The biological functions of the genes are shown by a color code. Pink stars indicate the genes also found associated with OS benefit (Figure 3). **D** and **E.** Venn diagrams showing the number and the name of genes associated with OS and/or PFS.

FFPE: Fixed Formalin Paraffin Embedded; H&E: Hematoxylin and Eosin; OS: Overall Survival; PFS: Progression Free Survival; HR: Hazard Ratio; CI: Confident Interval; CDS: CeDiranib Sensitive; CDInS: CeDiranib Insensitive.

Figure S3 (Related to Figure 4)

A. Global hierarchical clustering analysis identified co-expressed CDS and CDInS genes. **B.** Patients stratification based on CDS genes only. **C.** Patients stratification based on CDInS genes only. **D.** Kaplan-Meier curves and Cox regression analyses comparing the effect of chemo-plac and chemo-ced in patients with high and low expression of CDS genes on PFS.

E. Kaplan-Meier curves and Cox regression analyses comparing the effect of chemo-plac and chemo-ced in patients with high and low expression of CDInS genes on PFS.

HR: Hazard Ratio; CI: Confident Interval; CDS: CeDiranib Sensitive; CDInS: CeDiranib Insensitive.

Figure S4 (Related to Figure 5)

A-E. Heat maps showing gene expression changes in response to cediranib *in vivo*. **F.** PCA (Principal Component Analyse) of the xenograft models treated or not with cediranib based on metabolic gene expression level. **G.** Xenograft models information.

FC: Fold change

Figure S5 (Related to Figure 5 and 6)

A. Effect of Cediranib and/or FASNi treatment in Calu-6 and NCI-H526 xenograft models. **B.** Oxygen Consumption Rate in response to the Glycolytic test shown on Figure 6.D. **C.** Effect of glucose titration on proliferation of leptin treated Lovo cells. Lovo cells were treated with vehicle, leptin 10 ng/ml for 48 hours in serum free media. **D.** Western blot showing the protein accumulation for total and phospho-PDHE1a, total and phospho-S6 and beta-actin in response to leptin treatment. **E.** FASN staining in Lovo xenograft from mice treated with leptin +/- cediranib and quantification of the staining (**F**). **G.** Effect of leptin on cell proliferation in normoxia and hypoxic conditions. Cells were treated with vehicle, leptin 10 ng/ml for 48 hours in serum free media in normoxia and hypoxic conditions. t-test were used to determine significance and * indicates $P < 0.05$.

Figure S6 (Related to Figure 7)

A. B16F10 tumour growth curves in non-obese WT (Wild Type) and obese Db/Db mice treated with cediranib. **B.** Expression of genes involved in invasion, metastasis and inflammation in tumors from the non-obese WT (Wild Type) and obese Db/Db mice. t-tests

were used to determine significance and * indicates $P < 0.05$. C. Timing and number of mice taken out of study when tumors reached 1 cm^3 or showed signs of ulceration.

Figure S7 (Related to Figure 2, 3 and 4)

Summary diagram showing the factors associated with sensitivity and resistance to VEGFi treatment.

Table S1 (Related to Figure 1)

List of serum proteins and abbreviations.

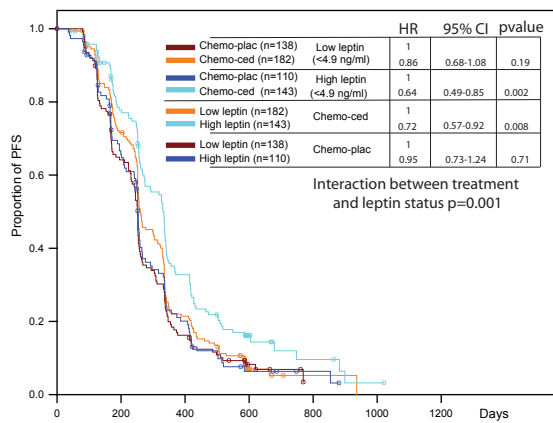
Table S2 (Related to Figure 3 and 4)

List, abbreviations and accession numbers of the genes analyzed by NanoString technology in mCRC patients (HORIZON II).

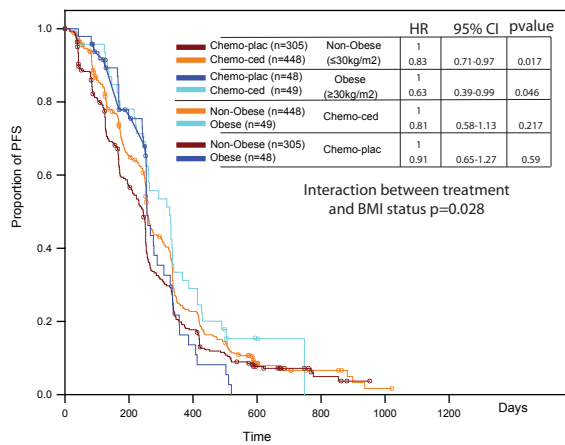
Table S3 (Related to Figure 5)

List, abbreviations, accession numbers and Applied Bioscience references of the genes analyzed by Taqman assays in xenograft models.

A

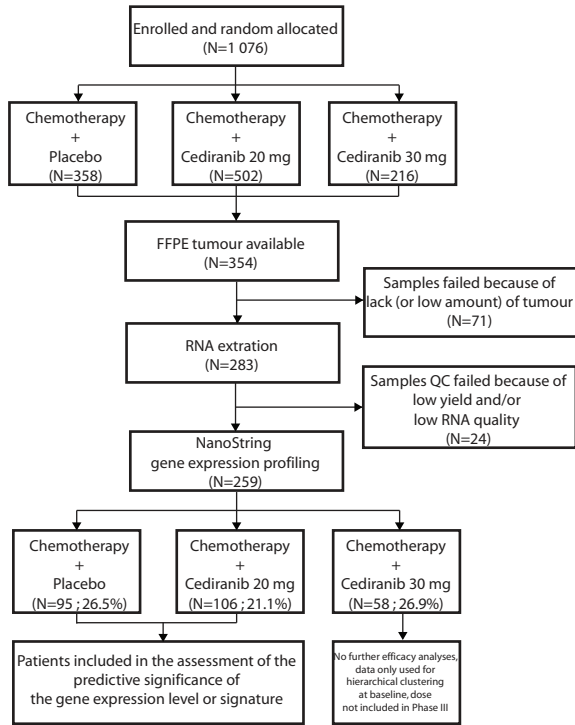


B

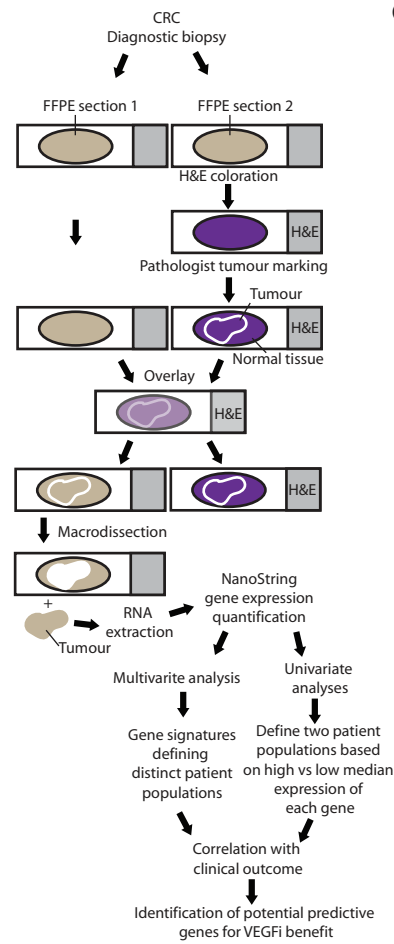


Pommier et al. Figure S1 (Related to Figure 2)

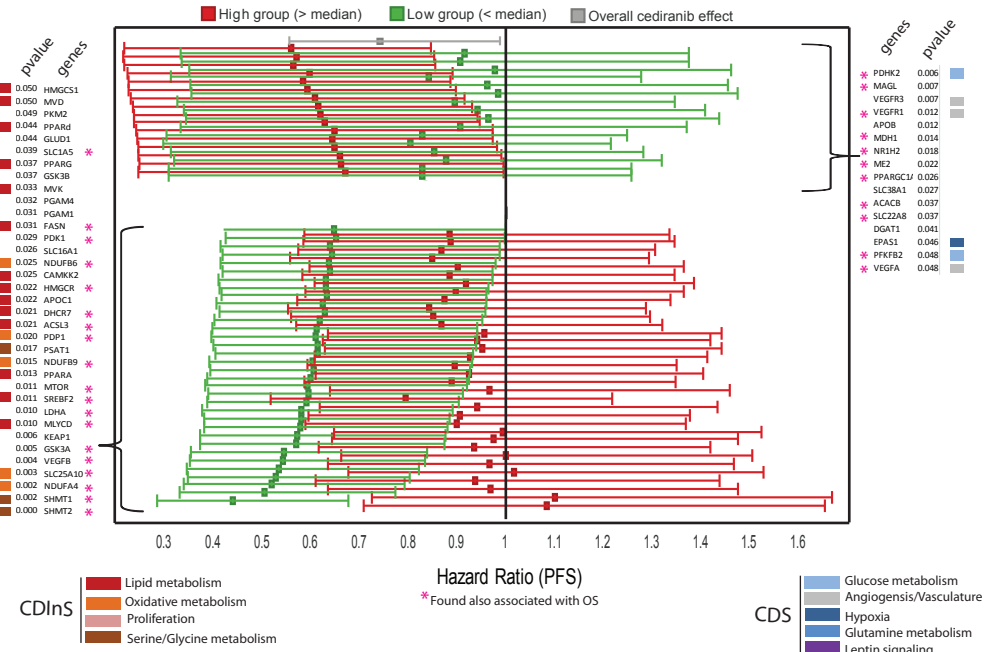
A



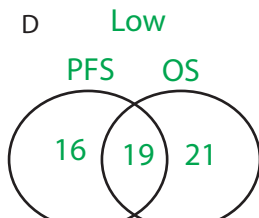
B



C

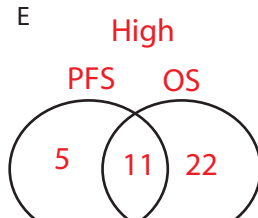


D

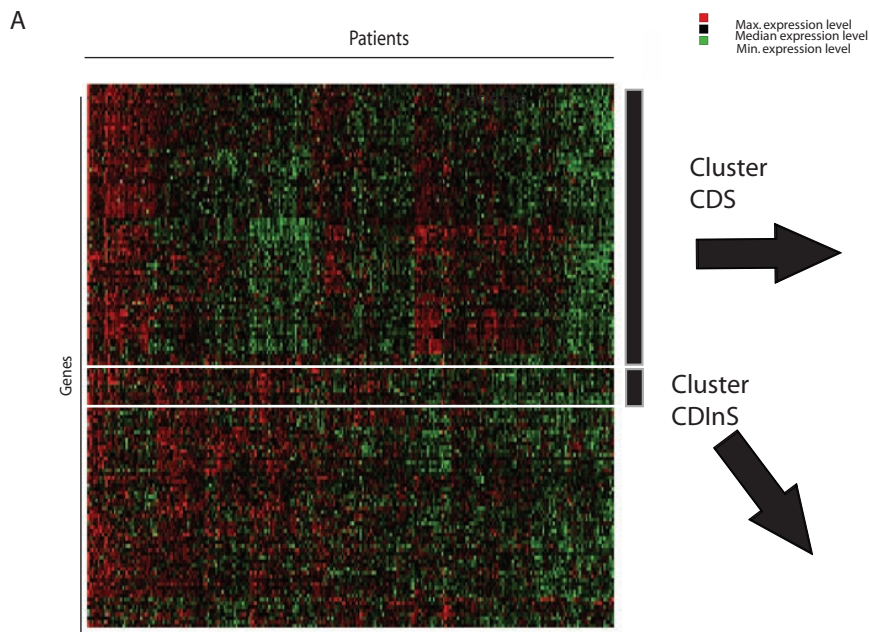


GSK3A SHMT2 LDHB
 KEAP1 NDUFB6 ACACA
 PPARA SLC25A10 TIGAR
 PSAT1 DHCR7 PCNA
 APOC1 HMGCR PDP2
 CAMKK2 FASN SCD
 SLC16A1 VEGFB NDUFC2
 PGAM1 MLYCD ENO1
 PGAM4 NDUFA4 NDU5B5
 MVK GSK3B SLC1A4
 PPARG PDK1 MKI67
 GLUD1 PDP1 GLS
 PPARG MTOR SLC38A7
 PKM2 SREBF2 ME3
 MVD SLC1A5 SLC16A3
 HMGCS1 NDUFB9 SOD1
 LDHA GFPT1
 SHMT1 PDK4
 ACSL3 CCND2
 FH
 G6PD

E

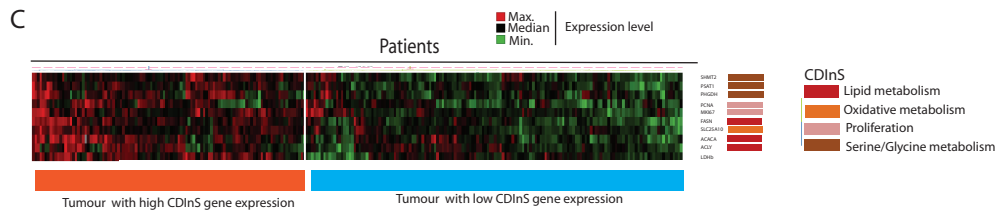
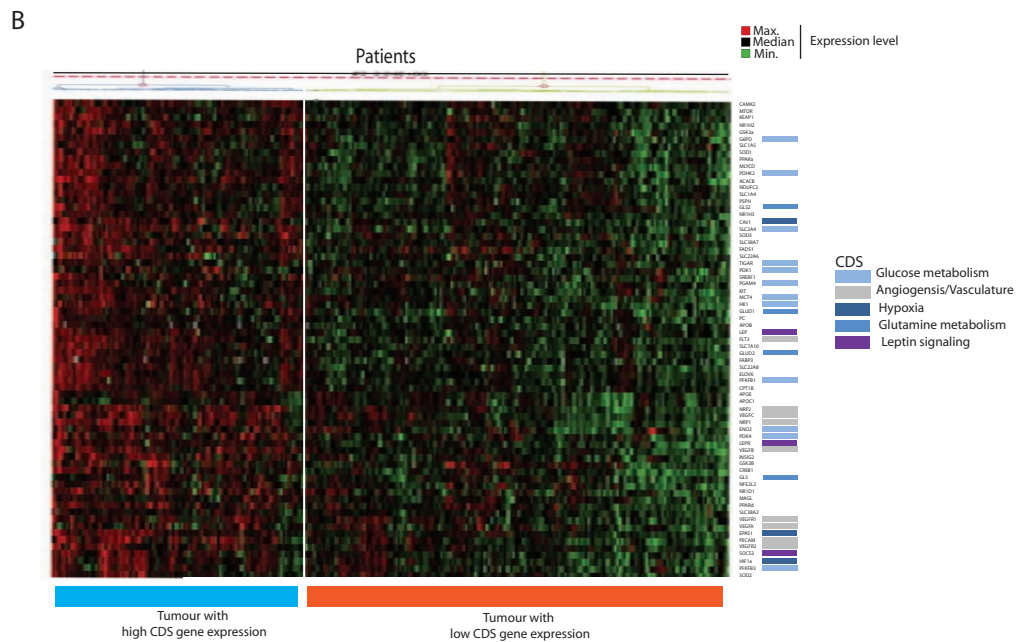


VEGFR3 VEGFR1 PCK1
 APOB NR1H2 NR1H3
 SLC38A1 PPARGC1A PFKFB3
 DGAT1 ACACB VEGFC
 EPAS1 PDHK2 CAV1
 MDH1 HIF1A
 HK1
 ME2 SLC38A2
 MAGL ELOVL6
 VEGFA SLC2A4
 PFKFB2 SLC2A4
 SLC22A8 CA9
 CREB1
 ACS2
 NFE2L2
 GLS2
 VEGFR2
 IDH2
 TIE1
 GLUD2
 GLUD1
 NRP2
 LEPR



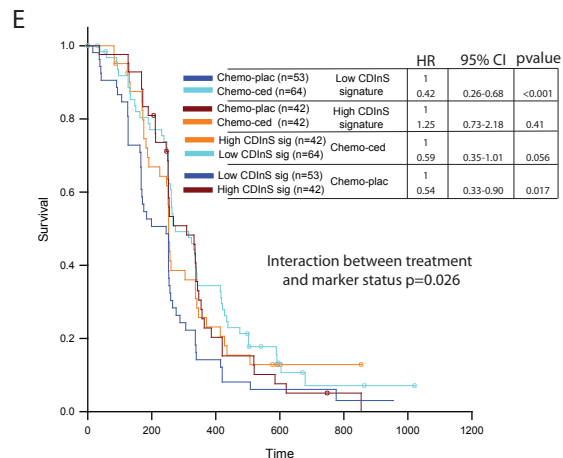
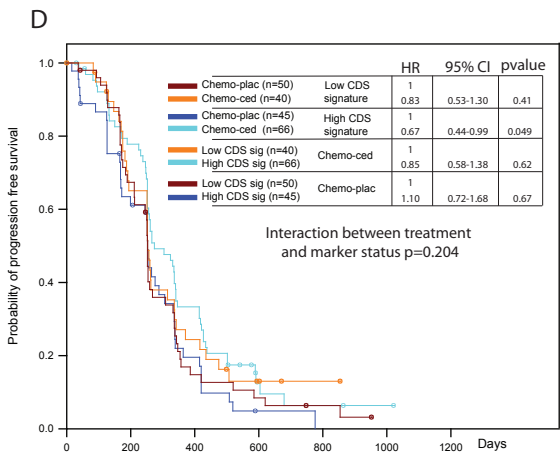
Global clustering

Identification of co-expressed gene clusters (CDS and CDInS)

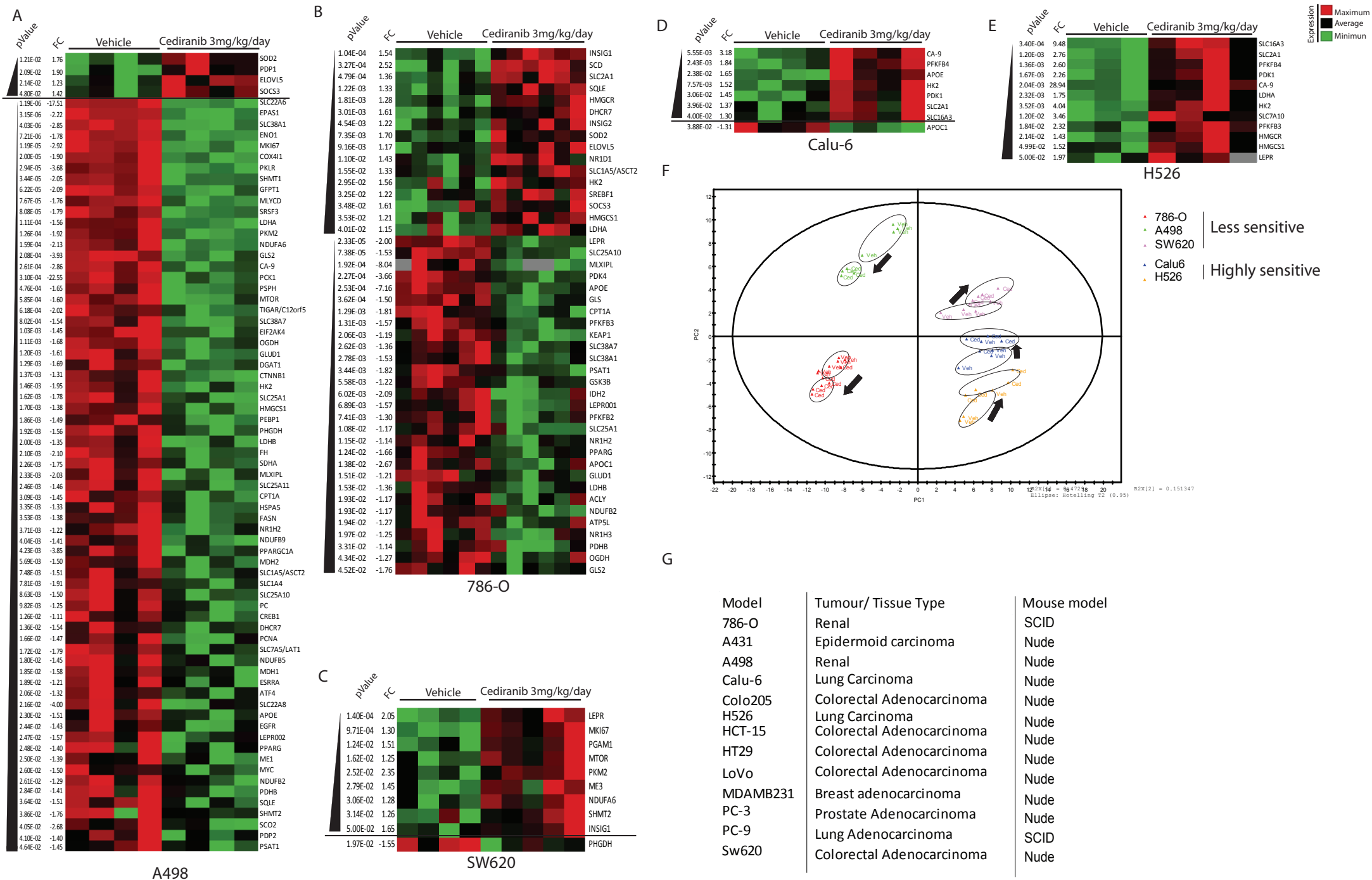


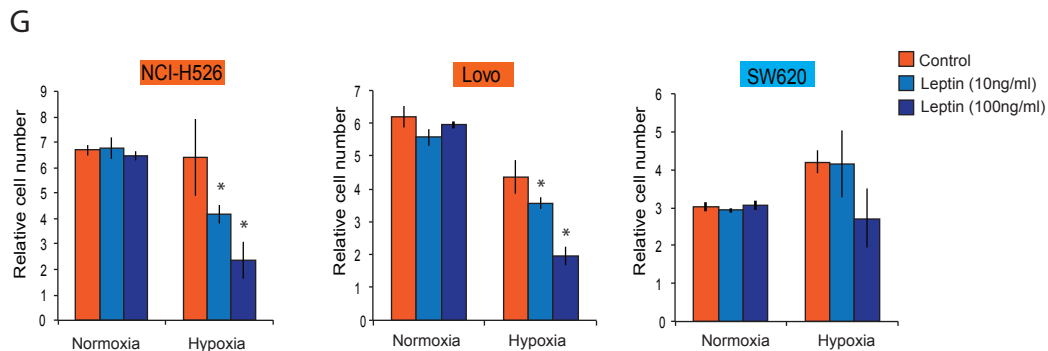
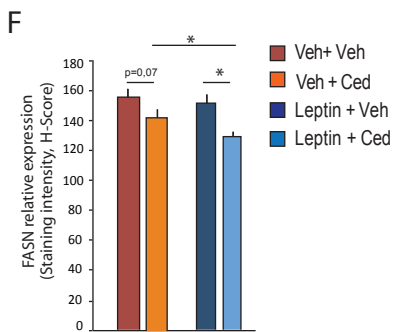
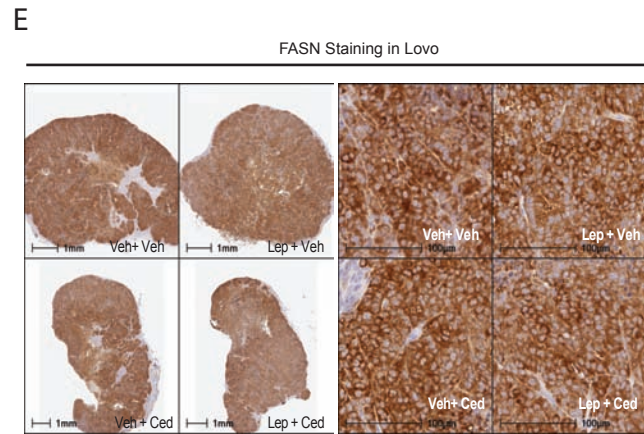
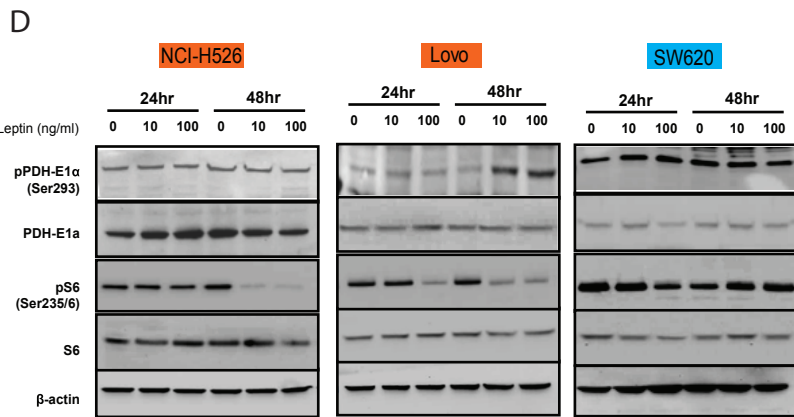
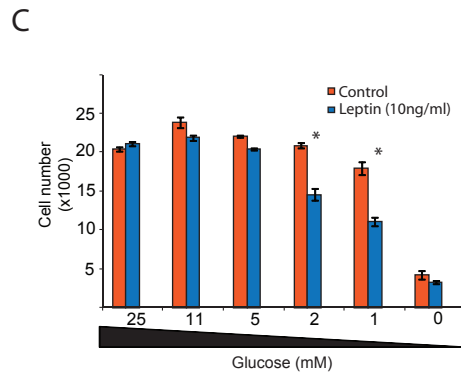
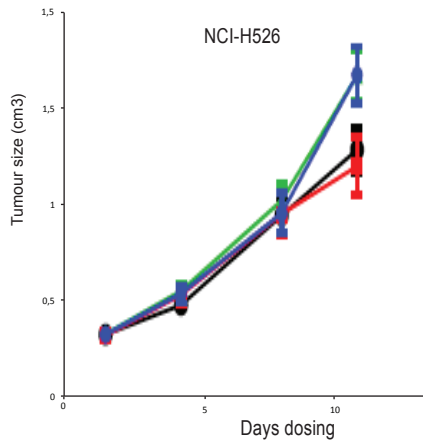
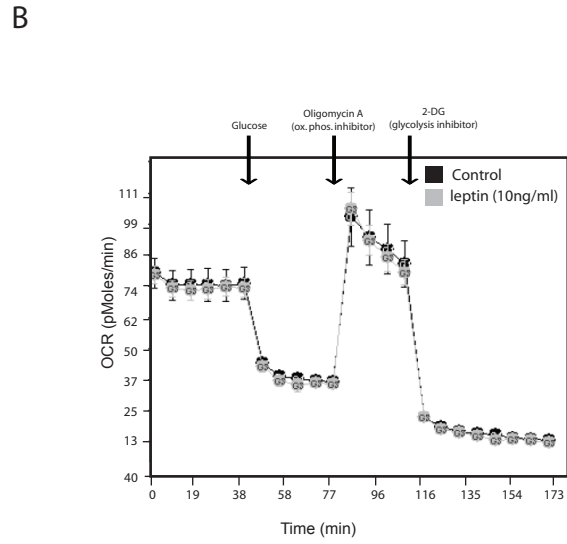
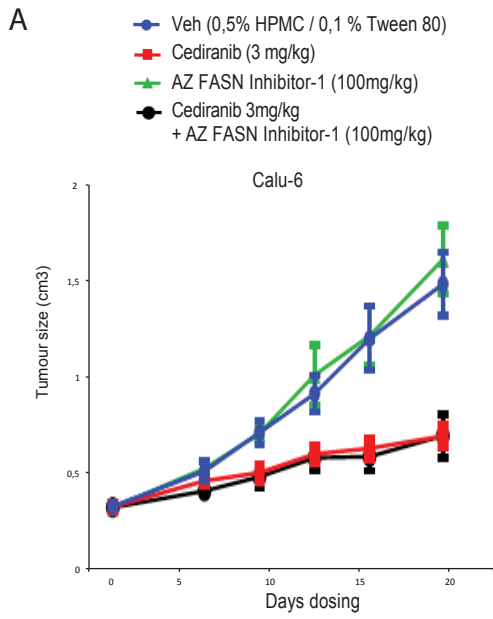
Refined clustering

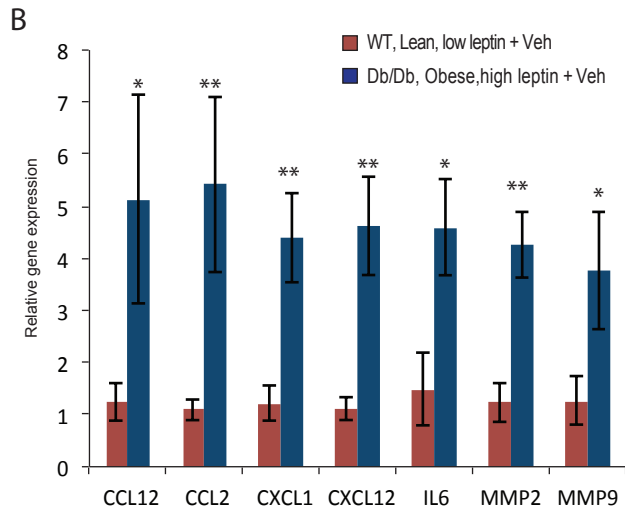
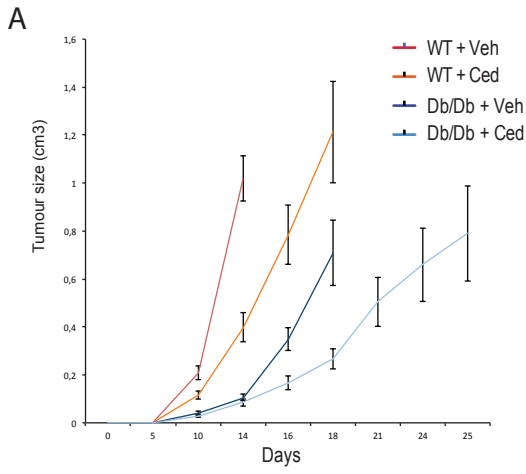
Patient stratification based on sub-clusters CDS and CDInS



Pommier et al. Figure S3 (Related to Figure 4)



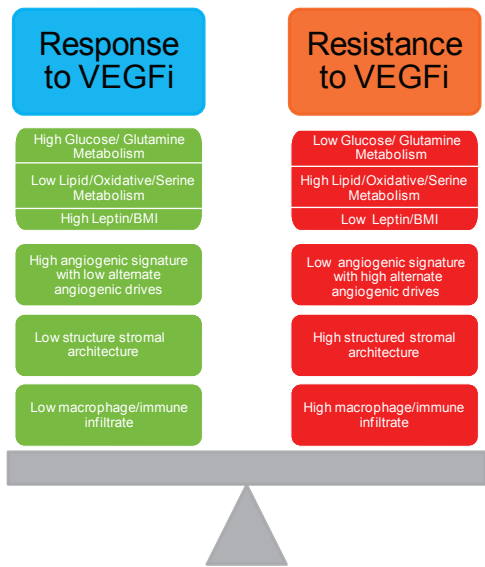




C

		Days on Study								
		13	14	15	16	17	18	21	24	25
WT + Vehicle	Tumor >1cm3		9		6					
	Ulcerated tumor									
WT + Cediranib	Tumor >1cm3				5		3			
	Ulcerated tumor						1			
Db/Db + Vehicle	Tumor >1cm3						1			
	Ulcerated tumor	1		1		5				
	PD analysis						6			
Db/Db + Cediranib	Tumor >1cm3								1	2
	Ulcerated tumor							1	1	1
	PD analysis						6			

Pommier et al. Figure S6 (Related to Figure 7)



Pommier et al. Figure S7 (Related to Figure 2, 3 and 4)

Biomarkers	Biomarker full name	Biomarkers	Biomarker full name
A2M	Alpha-2-Macroglobulin	IL-13	Interleukin 13
ACE	Angiotensin I Converting Enzyme (Peptidyl-Dipeptidase A) 1	IL-15	Interleukin 15
ACTH	Adrenocorticotrophic Hormone	IL-16	Interleukin 16
ADIPOQ	Adiponectin	IL-18	Interleukin 18
A-FABP	Fatty Acid-Binding Protein, Adipocyte	IL-1b	Interleukin 1b
AFP	Alpha-Fetoprotein	IL-1RA	Interleukin 1 Receptor Antagonist
AGER	Advanced Glycosylation End Product-Specific Receptor	IL-1α	Interleukin 1 Alpha
AgRP	Agouti-Related Protein	IL-2	Interleukin 2
AGT	Angiotensinogen	IL-25	Interleukin 25
Ang	Angiogenin, Ribonuclease, RNase A Family, 5	IL-2RA	Interleukin-2 Receptor, Alpha
Ang-2	Angiopoietin 2	IL-3	Interleukin 3
AREG	Amphiregulin	IL-4	Interleukin 4
AST	Aspartate Aminotransferase	IL-5	Interleukin 5
AXL-RTK	AXL Receptor Tyrosine Kinase	IL-6	Interleukin 6
B2M	Beta-2-Microglobulin	IL-6R	Interleukin 6 Receptor
BAFF	B Cell-Activating Factor	IL-6RB	Interleukin-6 Receptor Subunit Beta
BDNF	Brain-Derived Neurotrophic Factor	IL-7	Interleukin 7
BMP6	Bone Morphogenetic Protein 6	IL-8	Interleukin 8
BTC	Betacellulin	INFG	Interferon Gamma
CA 125	Carbohydrate Antigen 125	INS	Insulin
CA 15-3	Carbohydrate Antigen 15-3	KLK5	Kallikrein-Related Peptidase 5
CA 19-9	Carbohydrate Antigen 19-9	KLK7	Kallikrein-Related Peptidase 7
CA 72-4	Cancer Antigen 72-4	LEP	Leptin
CALB1	Calbindin 1, 28kDa	L-FABP	Fatty Acid-Binding Protein, Liver
CCL1	Chemokine (C-C Motif) Ligand 1	LGALS3BP	Lectin, Galactoside-Binding, Soluble, 3
CCL11	Chemokine (C-C Motif) Ligand 11	LH	Luteinizing Hormone
CCL13	Chemokine (C-C Motif) Ligand 13	Lp(a)	Lipoprotein (a)
CCL16	Chemokine (C-C Motif) Ligand 16	MB	Myoglobin
CCL19	Chemokine (C-C Motif) Ligand 19	M-CSF	Macrophage-Colony-Stimulating Factor
CCL2	Chemokine (C-C Motif) Ligand 2	MDA-LDL	Malondialdehyde-Modified Low Density Lipoprotein
CCL20	Chemokine (C-C Motif) Ligand 20	MICA	MHC Class I Polypeptide-Related Sequence A
CCL21	Chemokine (C-C Motif) Ligand 21	MIF	Macrophage Migration Inhibitory Factor
CCL22	Chemokine (C-C Motif) Ligand 22	MMP1	Matrix Metalloproteinase 1
CCL23	Chemokine (C-C Motif) Ligand 23	MMP10	Matrix Metalloproteinase 10
CCL24	Chemokine (C-C Motif) Ligand 24	MMP2	Matrix Metalloproteinase 2
CCL26	Chemokine (C-C Motif) Ligand 26	MMP3	Matrix Metalloproteinase 3
CCL3	Chemokine (C-C Motif) Ligand 3	MMP7	Matrix Metalloproteinase 7
CCL4	Chemokine (C-C Motif) Ligand 4	MMP9	Matrix Metalloproteinase 9
CCL7	Chemokine (C-C Motif) Ligand 7	MMP9f	Matrix Metalloproteinase 9, Free
CCL8	Chemokine (C-C Motif) Ligand 8	MPO	Myeloperoxidase
CD40L	CD40 Ligand	MRC2	Mannose Receptor, C Type 2
CD62E	E-Selectin	MSLN	Mesothelin
CEA	Carcinoembryonic Antigen	IMST1	Macrophage Stimulating 1 (Hepatocyte Growth Factor-Like)
CgA	Chromogranin A	NCAM	Neuronal Cell Adhesion Molecule
CHI3L1	Chitinase 3-Like 1 (Cartilage Glycoprotein-39)	NGF	Nerve Growth Factor (Beta Polypeptide)
c-Kit	Mast/Stem Cell Growth Factor Receptor	NRP1	Neuropilin 1
CK-MB	Creatine Kinase, MB	NT-proBNP	N-Terminal Pro-Brain Natriuretic Peptide
CLEC3B	C-Type Lectin Domain Family 3, Member B	OLR1	Oxidized Low Density Lipoprotein (Lectin-Like) Receptor 1
CLU	Clusterin	OPN	Osteopontin
CNF	Ciliary Neurotrophic Factor	PAI-1	Plasminogen-Activator-Inhibitor-1
COL15A1	Collagen, Type XVIII, Alpha 1	PAP	Prostatic Acid Phosphatase
COL4	Collagen, Type IV	PAPPA	Pregnancy-Associated Plasma Protein A, Pappalysin 1
CRP	C-Reactive Protein	PDGF-BB	Platelet-Derived Growth Factor BB
CSF2	Colony-Stimulating Factor 2	PGA	pepsinogen I
CT	Calcitonin	PGF	Placental Growth Factor
CTGF	Connective Tissue Growth Factor	PLAU	Plasminogen Activator, Urokinase
CTSD	Cathepsin D	PP	Pancreatic Polypeptide
CXCL1	Chemokine (C-X-C Motif) Ligand 1	PRL	Prolactin
CXCL10	Chemokine (C-X-C Motif) Ligand 10	PRS	Prostasin
CXCL11	Chemokine (C-X-C Motif) Ligand 11	PSA	Prostate Specific Antigen, Free
CXCL12	Chemokine (C-X-C Motif) Ligand 12	PYY	Peptide YY
CXCL13	Chemokine (C-X-C Motif) Ligand 13	RANTES	T-Cell-Specific Protein RANTES
CXCL5	Chemokine (C-X-C Motif) Ligand 5	RETN	Resistin
CXCL9	Chemokine (C-X-C Motif) Ligand 9	S100-A12	S100 Calcium Binding Protein A12
EGF	Epidermal Growth Factor	S100B	S100B
EGFR	Epidermal Growth Factor Receptor	SAP	Amyloid P Component, Serum
ENG	Endoglin, Quant	SCF	Stem Cell Factor
EpCAM	Epithelial Cell Adhesion Molecule	SCT	Secretin
EPO	Erythropoietin	SERPINB5	Maspin
EPR	Epregrin	SHBG	Sex Hormone Binding Globulin
ERBB3	Erythroblastic Leukemia Viral Onco H3	SOD1	Superoxide Dismutase 1, Soluble
ET-1	Endothelin 1	SORT1	Sortilin 1
FASLG	Fas Ligand (TNF Superfamily, Member 6)	TBG	Thyroxine Binding Globuline
FB1-1C	Fibulin-1C	Tg	Thyroglobulin
FGF2	Basic Fibroblast Growth Factor	TGF-α	Transforming Growth Factor, Alpha
FGF4	Fibroblast Growth Factor 4	TGF-β1	Transforming Growth Factor, Beta 1
FGF3	Fibroblast Growth Factor 3	TGF-β3	Transforming Growth Factor, Beta 3
FN	Cellular Fibronectin	THBS1	Thrombospondin 1
FSH	Follicle Stimulating Hormon	THPO	Thrombopoietin
FT	Ferritin	TIE-2	Receptor Tyrosine Kinase, Endothelial, TIE-2
FVII	Factor VII Concentration	TIMP1	TIMP Metalloproteinase Inhibitor 1
GCSF	Colony Stimulating Factor 3 (Granulocyte)	TM	Thrombomodulin
GH	Growth Hormone	TNC	Tenascin C
GLP-1	Glucagon-Like Peptide 1, Total	TNF-α	Tumor Necrosis Factor, Alfa
GSN	Gelsolin	TNF-β	Tumor Necrosis Factor, Beta
GST	Glutathione S-Transferase Alpha	TNFR1	Tumor Necrosis Factor Receptor-Like 2
HAVCR1	Hepatitis A Virus Cellular Receptor 1	TNFR	Tumor Necrosis Factor Receptor Type I
HB-EGF	Heparin-Binding EGF-Like Growth Factor	TNFRSF6	Fas (TNF Receptor Superfamily, Member 6)
HE4	Human Epididymis Protein 4	TNFRSF5	Tumor Necrosis Factor Recept, Superfam5
HER2	Human Epidermal Growth Factor Receptor 2	TNFRSF11	Tumor Necrosis Factor Receptor Superfamily, Member 11B
hFABP	Heart-Type Fatty Acid-Binding Protein	t-PA	Tissue Plasminogen Activator antigen
HGF	Hepatocyte Growth Factor	TRAILR3	TNF-Related Apoptosis-Inducing Ligand Receptor 3
HGFR	Met Proto-Oncogene (Hepatocyte Growth Factor Receptor)	TSH	Thyroid Stimulating Hormone
HNL	Human Neutrophil Lipocaline	VCAM1	Vascular Cell Adhesion Molecule 1
HPN	Hepsin	VEGFA	Vascular Endothelial Growth Factor
ICAM1	Intercellular Adhesion Molecule-1	VEGFB	Vascular Endothelial Growth Factor B
IgE	Immunoglobulin E	VEGFC	Vascular Endothelial Growth Factor C
IGF-1	Insulin-Like Growth Factor 1	VEGFD	Vascular Endothelial Growth Factor D
IGFBP1	Insulin-Like Growth Factor Bind. Prot 1	VEGFR1	FMS-Related Tyrosine Kinase 1
IGFBP2	Insulin-Like Growth Factor Bind. Prot 2	VEGFR2	Kinase Insert Domain Receptor
IL-10	Interleukin 10	VEGFR3	Fms-Related Tyrosine Kinase 4
IL-11	Interleukin 11	vWF	von Willebrand Factor
IL-12p40	Interleukin 12 (p40)	XL1	Chemokine (C Motif) Ligand 1
IL-12p70	Interleukin 12 (p70)		

Pommier et al. Table S1 (Related to Figure 1)
List of serum proteins and abbreviations.

General pathway	Gene name	Gene full name	Accession number
Amino acids metabolism	SLC1A4	solute carrier family 1 (glutamate/neutral amino acid transporter), member 4	NM_00308.4:3030
	SLC1A5/ASCT2	solute carrier family 1 (neutral amino acid transporter), member 5	NM_001451444:1489
	SLC38A1	solute carrier family 38, member 1	NM_001077841:5825
	SLC38A2	solute carrier family 38, member 2	NM_018976.4:1170
	SLC38A7	solute carrier family 38, member 7	NM_018231.1:1810
	SLC7A10	solute carrier family 7 (neutral amino acid transporter light chain, asc system), member 10	NM_019849.2:1470
	SLC7A5/LAT1	solute carrier family 7 (amino acid transporter light chain, L system), member 5	NM_003486.5:785
	SLC22A6	solute carrier family 22 (organic anion transporter), member 6	NM_004790.3:900
	SLC22A8	solute carrier family 22 (organic anion transporter), member 8	NM_004254.3:1170
	Proliferation	CCND2	cyclin D2
NRK17		antigen identified by monoclonal antibody Ki-67	NM_002417.0:4020
PCNA		proliferating cell nuclear antigen	NM_002592.2:390
PK1		phosphoenolpyruvate carboxylase 1 (soluble)	NM_002591.2:1870
Glucose metabolism	SLC2A1	solute carrier family 2 (facilitated glucose transporter), member 1	NM_005616.2:2500
	SLC2A4	solute carrier family 2 (facilitated glucose transporter), member 4	NM_001042.2:2120
	ENO1	enolase 1, (alpha)	NM_001428.2:1689
	ENO2	enolase 2	NM_001975.2:1855
	G6PD	glucose-6-phosphate dehydrogenase	NM_000402.2:1155
	HK1	hexokinase 1	NM_000188.2:3355
	HK2	hexokinase 2	NM_000189.2:6880
	PDHK2	pyruvate dehydrogenase kinase, isozyme 2	NM_002611.3:435
	PDHK3	pyruvate dehydrogenase kinase, isozyme 3	NM_003391.1:585
	PDK1	pyruvate dehydrogenase kinase, isozyme 1	NM_002610.3:1170
	PDK4	pyruvate dehydrogenase kinase, isozyme 4	NM_002612.3:1675
	PFKFB1	6-phosphofructo-2-kinase/fructose-2,6-bisphosphatase 1	NM_002625.2:564
	PFKFB2	6-phosphofructo-2-kinase/fructose-2,6-bisphosphatase 2	NM_001018053.1:445
	PFKFB3	6-phosphofructo-2-kinase/fructose-2,6-bisphosphatase 3	NM_001145443.1:495
	PFKFB4	6-phosphofructo-2-kinase/fructose-2,6-bisphosphatase 4	NM_004567.2:400
	PFKAN1	phosphoglycerate mutase 1 (brain)	NM_002629.2:1037
	PFKAN4	phosphoglycerate mutase family member 4	NM_001029891.2:1207
	PKMD	pyruvate kinase, muscle	NM_182471.1:2105
	TIGAR	Tp53-induced glycolysis and apoptosis regulator	NM_003075.2:5245
	Glutamine metabolism	LDHA	lactate dehydrogenase A
LDHB		lactate dehydrogenase B	NM_001174097.1:1190
SLC16A1		solute carrier family 16, member 1 (monocarboxylic acid transporter 1)	NM_003051.3:635
SLC16A3		solute carrier family 16, member 3 (monocarboxylic acid transporter 4)	NM_004207.2:370
GFPT1		glutamine--fructose-6-phosphate transaminase 1	NM_001244710.1:606
GLS		glutaminase	NM_014905.3:585
GLS2		glutaminase 2 (liver, mitochondrial)	NM_001367.2:1945
GLUD1		glutamate dehydrogenase 1	NM_005271.2:2680
GLUD2		glutamate dehydrogenase 2	NM_012084.3:13
IDH1		isocitrate dehydrogenase 1 (NADP+), soluble	NM_005896.2:105
Hypoxia	CA-9	Carbonic anhydrase 9	NM_001216.2:960
	CAV1	caveolin 1, caveolae protein, 22kDa	NM_001753.3:434
	EPAS1	endothelial PAS domain protein 1	NM_001430.3:4246
	HIF1A	hypoxia inducible factor 1, alpha subunit (basic helix-loop-helix transcription factor)	NM_001530.2:1985
Leptin signaling	SOCS3	suppressor of cytokine signaling 3	NM_005955.3:1870
	LEP	leptin	NM_002302.2:1875
Lipid metabolism	LEPR	leptin receptor	NM_001003679.1:2000
	DHCR7	7-dehydrocholesterol reductase	NM_001360.2:780
	HMGCR	3-hydroxy-3-methylglutaryl-CoA reductase	NM_000859.2:3905
	HMGCS1	3-hydroxy-3-methylglutaryl-CoA synthase 1 (soluble)	NM_002130.4:420
	MVD	Mevalonate (Diphospho) Decarboxylase	NM_002461.1:128
	MVK	Mevalonate Kinase	NM_000431.2:201
	SOLE	squalene epoxidase	NM_001129.3:250
	ACACA	acetyl-CoA carboxylase alpha	NM_138834.1:3681
	ACACB	acetyl-CoA carboxylase beta	NM_000983.3:3865
	ACLY	ATP citrate lyase	NM_001096.2:3195
	ACSS2	acyl-CoA synthetase short-chain family member 2	NM_001076552.2:655
	DGAT1	diacylglycerol O-acyltransferase 1	NM_012079.4:544
	ELOVL5	ELOVL fatty acid elongase 5	NM_001242831.1:46
	ELOVL6	ELOVL fatty acid elongase 6	NM_001130721.1:1035
	FADS1	fatty acid desaturase 1	NM_0013402.3:1560
	FASN	fatty acid synthase	NM_004104.4:5387
	MLYCD	malonyl-CoA decarboxylase	NM_002213.2:1530
	SCD	stearyl-CoA desaturase (delta-9-desaturase)	NM_005063.3:2025
	ACSL3	Acyl-CoA Synthetase Long-Chain Family Member 3	NM_003371.2:2210
	CPT1A	carnitine palmitoyltransferase 1A (liver)	NM_001876.3:1355
CPT1B	carnitine palmitoyltransferase 1B (muscle)	NM_004377.3:2578	
MAGL	Monoglyceride Lipase	NM_001283.5:1355	
APOB	apolipoprotein B (including Ag(x) antigen)	NM_000384.2:2833	
APOC1	apolipoprotein C-I	NM_001645.3:270	
APOE	apolipoprotein E	NM_000041.2:96	
SREBF1	sterol regulatory element binding transcription factor 1	NM_001005291.1:1392	
SREBF2	sterol regulatory element binding transcription factor 2	NM_004599.2:4080	
FABP3	fatty acid binding protein 3	NM_004023.3:915	
COX4I1	cytochrome c oxidase subunit IV isoform 1	NM_001861.2:160	
Cs	citrate synthase	NM_004077.2:740	
FH	fumarate hydratase	NM_000143.2:203	
IDH2	isocitrate dehydrogenase 2 (NADP+), mitochondrial	NM_002168.2:944	
MDH1	malate dehydrogenase 1, NAD (soluble)	NM_005917.3:970	
MDH2	malate dehydrogenase 2, NAD (mitochondrial)	NM_005918.2:475	
ME1	malic enzyme 1, NAD(P)+-dependent, cytosolic	NM_002395.3:1405	
ME2	malic enzyme 2, NAD(P)+-dependent, mitochondrial	NM_002396.3:610	
ME3	malic enzyme 3, NAD(P)+-dependent, mitochondrial	NM_001014811.1:1080	
NDUFA4	NADH dehydrogenase (ubiquinone) 1 alpha subcomplex, 4, 9kDa	NM_002489.2:35	
NDUFA6	NADH dehydrogenase (ubiquinone) 1 alpha subcomplex, 6, 14kDa	NM_002490.3:430	
NDUFB2	NADH dehydrogenase (ubiquinone) 1 beta subcomplex, 2, 8kDa	NM_004546.2:230	
NDUFB4	NADH dehydrogenase (ubiquinone) 1 beta subcomplex, 4, 15kDa	NM_004547.2:254	
NDUFB5	NADH dehydrogenase (ubiquinone) 1 beta subcomplex, 5, 16kDa	NM_002492.3:115	
NDUFB6	NADH dehydrogenase (ubiquinone) 1 beta subcomplex, 6, 17kDa	NM_001199987.1:9	
NDUFB9	NADH dehydrogenase (ubiquinone) 1 beta subcomplex, 9, 22kDa	NM_005005.2:80	
NDUFC2	NADH dehydrogenase (ubiquinone) 1, subcomplex unknown, 2, 14.5kDa	NM_001240541.1:1235	
OGDH	oxoglutarate (alpha-ketoglutarate) dehydrogenase (lipoamide)	NM_002541.2:65	
PC	pyruvate carboxylase	NM_002003.3:2055	
PDHB	pyruvate dehydrogenase (lipoamide) beta	NM_000925.3:555	
PDP1	pyruvate dehydrogenase phosphatase catalytic subunit 1	NM_001161778.1:950	
PDP2	pyruvate dehydrogenase phosphatase catalytic subunit 2	NM_0020786.2:6505	
SDHA	succinate dehydrogenase complex, subunit A, flavoprotein (Fp)	NM_004168.1:230	
SLC25A1	solute carrier family 25 (mitochondrial carrier, citrate transporter), member 1	NM_005984.2:964	
SLC25A10	solute carrier family 25 (mitochondrial carrier, dicarboxylate transporter), member 10	NM_0012140.3:390	
SLC25A11	solute carrier family 25 (mitochondrial carrier, oxoglutarate carrier), member 11	NM_003562.4:860	
HNF4A	hepatocyte nuclear factor 4, alpha	NM_178850.1:1116	
KAP1	ketch-like CCH-associated protein 1	NM_000899.3:561	
NFE2L2/nrf2	nuclear factor (erythroid-derived 2)-like 2	NM_006164.4:746	
SOD1	superoxide dismutase 1, soluble	NM_000454.4:35	
SOD2	superoxide dismutase 2, mitochondrial	NM_000636.2:640	
SOD3	superoxide dismutase 3, extracellular	NM_003102.2:1135	
CAMKK2	calcium/calmodulin-dependent protein kinase kinase 2, beta	NM_005449.3:1710	
CREB1	cAMP responsive element binding protein 1	NM_134442.2:200	
ENTPD5	Ectonucleoside Triphosphate Diphosphohydrolase 5	NM_001249.2:1585	
PEBP1	phosphatidylethanolamine binding protein 1	NM_002567.2:1335	
GSK3A	glycogen synthase kinase 3 alpha	NM_001984.2:480	
GSK3B	glycogen synthase kinase 3 beta	NM_002093.2:925	
INSIG1	insulin induced gene 1	NM_005542.3:1120	
INSIG2	insulin induced gene 2	NM_016133.2:513	
MLXIPL	MLX interacting protein-like	NM_032951.2:2805	
MTOR	mechanistic target of rapamycin (serine/threonine kinase)	NM_004958.2:5095	
MYC	v-myc myelocytomatosis viral oncogene homolog (avian)	NM_002467.3:1610	
NR1D1	nuclear receptor subfamily 1, group D, member 1	NM_021724.3:1080	
NR1H2	nuclear receptor subfamily 1, group H, member 2	NM_007121.3:40	
NR1H3	nuclear receptor subfamily 1, group H, member 3	NM_005693.2:1575	
PPARA	peroxisome proliferator-activated receptor alpha	NM_001010928.2:5200	
PPARD	peroxisome proliferator-activated receptor delta	NM_006238.4:107	
PPARG	peroxisome proliferator-activated receptor gamma	NM_015869.3:1035	
PPARGCIA	peroxisome proliferator-activated receptor gamma, coactivator 1 alpha	NM_013261.3:1505	
Serine/glycine synthesis	PHGDH	phosphoglycerate dehydrogenase	NM_006233.3:1900
	PSAT1	phosphoserine aminotransferase 1	NM_021154.3:1445
	PSPH	phosphoserine phosphatase	NM_004577.3:225
	SHMT1	serine hydroxymethyltransferase 1 (soluble)	NM_148918.1:1800
SHMT2	serine hydroxymethyltransferase 2 (mitochondrial)	NM_001166356.1:1480	
Angiogenesis/Vasculature	FLT1	fms-related tyrosine kinase 1 (vascular endothelial growth factor/vascular permeability factor receptor)	NM_002019.4:530
	FLT3	fms-related tyrosine kinase 3	NM_004119.1:580
	FLT4	fms-related tyrosine kinase 4	NM_002020.1:955
	KDR	kinase insert domain receptor (a type III receptor tyrosine kinase)	NM_002253.2:1420
	NRP1	neuropilin 1	NM_003873.5:370
	NRP2	neuropilin 2	NM_003872.2:805
	PECAM1	platelet/endothelial cell adhesion molecule 1	NM_000442.3:1365
	TIE1	tyrosine kinase with immunoglobulin-like and EGF-like domains 1	NM_00524.2:2610
	VEGFA	vascular endothelial growth factor A	NM_001025366.1:1325
	VEGFB	vascular endothelial growth factor B	NM_003377.3:687
VEGFC	vascular endothelial growth factor C	NM_005429.2:565	
Housekeeping	RPLP0	ribosomal protein, large, P0	NM_001002.3:250
	RPL19	ribosomal protein L19	NM_000981.3:645
	PGK1	phosphoglycerate kinase 1	NM_000291.2:1030
	GAPDH	glyceraldehyde-3-phosphate dehydrogenase	NM_002046.3:104
	CTC	clathrin, heavy chain	NM_004859.2:290
	BDM	beta-2-microglobulin	NM_004048.2:25
ACTB	actin, beta	NM_001011.2:1010	

Pommier et al. Table S2 (Related to Figure 3 and 4): List, abbreviations and accession numbers of the genes analyzed by NanoString technology in mCRC patients (HORIZON II).

Metab functions	Gene Symbol	Fluidigm	Full gene name	Accession number	Human specific assay ID
Amino acids transport	SLC1A4		solute carrier family 1 (glutamate/neutral amino acid transporter), member 4	NM_003038.4:3030	HS01046029_m1
	SLC1A5/ASCT2		solute carrier family 1 (neutral amino acid transporter), member 5	NM_001145144.1:1180	HS00153715_m1
	SLC38A1		solute carrier family 38, member 1	NM_001077484.1:5825	HS01071209_m1
	SLC38A2		solute carrier family 38, member 2	NM_018976.4:1170	HS03037377_m1
	SLC38A7		solute carrier family 38, member 7	NM_018231.1:1810	HS00171168_m1
	SLC7A10		solute carrier family 7 (neutral amino acid transporter light chain, asc system), member 10	NM_019849.2:1470	HS00982744_m1
	SLC7A5/LAT1		solute carrier family 7 (amino acid transporter light chain, L system), member 5	NM_003486.5:785	HS01120918_m1
	SLC22A6		solute carrier family 22 (organic anion transporter), member 6	NM_004790.3:900	HS00909569_g1
	SLC22A8		solute carrier family 22 (organic anion transporter), member 8	NM_004254.3:1170	HS00758883_s1
	CCND2		cyclin D2	NM_001759.2:5825	HS00608644_m1
Cell cycle	MKI67		antigen identified by monoclonal antibody Ki-67	NM_002417.2:4020	HS00154208_m1
	PCNA		proliferating cell nuclear antigen	NM_002592.2:280	HS00902177_m1
Glucose metabolism	PFK1		phosphoenolpyruvate carboxykinase 1 (soluble)	NM_002591.2:1870	HS00264683_m1
	ENO1		enolase 1, [alpha]	NM_001428.2:1689	HS00936368_m1
	G6PD		glucose-6-phosphate dehydrogenase	NM_000402.2:1155	HS00855332_g1
	HK1		hexokinase 1	NM_000188.2:3355	HS01032072_m1
	HK2		hexokinase 2	NM_000189.4:6880	HS01034055_g1
	PDK1		pyruvate dehydrogenase kinase, isozyme 1	NM_002610.3:1170	HS00168352_m1
	PDK4		pyruvate dehydrogenase kinase, isozyme 4	NM_002612.3:1675	HS00940429_m1
	PFKFB1		6-phosphofructo-2-kinase/fructose-2,6-bisphosphatase 1	NM_002625.2:564	HS04260079_mH
	PFKFB2		6-phosphofructo-2-kinase/fructose-2,6-bisphosphatase 2	NM_001018053.1:445	HS00946084_g1
	PFKFB3		6-phosphofructo-2-kinase/fructose-2,6-bisphosphatase 3	NM_001145443.1:495	HS01855675_s1
	PFKFB4		6-phosphofructo-2-kinase/fructose-2,6-bisphosphatase 4	NM_004567.2:400	HS00946379_m1
	PGAM1		phosphoglycerate mutase 1 (brain)	NM_002629.2:1037	HS01650979_m1
	PGAM4		phosphoglycerate mutase family member 4	NM_001038891.2:1207	HS01013986_m1
	PKM2		pyruvate kinase, muscle	NM_182471.1:2305	HS01033432_m1
	TIGAR		Tp53-induced glycolysis and apoptosis regulator	NM_020375.2:2345	HS00947539_m1
	LDHA		lactate dehydrogenase A	NM_005566.1:985	HS00902244_m1
	LDHB		lactate dehydrogenase B	NM_001174097.1:1190	HS00155110_m1
	SLC16A1		solute carrier family 16, member 1 (monocarboxylic acid transporter 1)	NM_003051.3:635	HS00938919_m1
	SLC2A1		solute carrier family 2 (facilitated glucose transporter), member 1	NM_005516.2:2500	HS00950073_g1
	SLC2A4		solute carrier family 2 (facilitated glucose transporter), member 4	NM_001042.2:2120	HS00896610_m1
SLC16A3		solute carrier family 16, member 3 (monocarboxylic acid transporter 4)	NM_004207.2:370	HS00938109_m1	
Glutamine metabolism	GFPT1		glutamine-fructose-6-phosphate transaminase 1	NM_001244710.1:606	HS01014019_m1
	GLS		glutaminase	NM_014505.3:985	HS00987287_g1
	GLS2		glutaminase 2 (liver, mitochondrial)	NM_013267.2:1945	HS01632647_g1
	GLUD1		glutamate dehydrogenase 1	NM_005271.2:2680	HS01649931_s1
	GLUD2		glutamate dehydrogenase 2	NM_012084.3:13	HS00979738_m1
	IDH1		isocitrate dehydrogenase 1 (NADP+), soluble	NM_005896.2:105	HS01047720_m1
	CA-9		Carbonic anhydrase 9	NM_001216.2:960	HS00174877_m1
	CAV1		caveolin 1, caveolae protein, 22kDa	NM_001753.3:434	HS04260076_g1
	EPAS1		endothelial PAS domain protein 1	NM_001430.3:426	HS00174497_m1
	HIF1A		hypoxia inducible factor 1, alpha subunit (basic helix-loop-helix transcription factor)	NM_001530.2:1885	HS00906383_m1
Leptin signaling	SOS3		suppressor of cytokine signaling 3	NM_003955.3:1870	HS00751507_s1
	LEP		leptin	NM_000230.2:1875	HS00244618_m1
LEPR			leptin receptor	NM_001003679.1:2000	HS01055263_g1
				NM_198834.1:3681	HS02574374_s1
Lipid metabolism	ACACA		acetyl-CoA carboxylase alpha	NM_001093.3:3365	HS00355045_m1
	ACACB		acetyl-CoA carboxylase beta	NM_001096.2:3195	HS00201385_m1
	ACLY		ATP citrate lyase	NM_001076552.2:655	HS01023087_m1
	ACS2		acyl-CoA synthetase short-chain family member 2	NM_012079.4:544	HS00361415_m1
	DGAT1		diacylglycerol O-acyltransferase 1	NM_001242831.1:46	HS01010957_m1
	ELOVL5		ELOVL fatty acid elongase 5	NM_001130721.1:1035	HS01094707_m1
	ELOVL6		ELOVL fatty acid elongase 6	NM_004104.4:5387	HS04260288_m1
	FASN		fatty acid synthase	NM_0012213.2:1530	HS01026142_m1
	MLYCD		malonyl-CoA decarboxylase	NM_005063.4:2025	HS00174860_m1
	SCD		stearoyl-CoA desaturase (delta-9-desaturase)	NM_001876.3:1355	HS01067158_gH
	CPT1A		carnitine palmitoyltransferase 1A (liver)	NM_004377.3:2578	HS01056622_m1
	CPT1B		carnitine palmitoyltransferase 1B (muscle)	NM_001360.2:780	HS00971639_m1
	DHCR7		7-dehydrocholesterol reductase	NM_000859.2:3905	HS00971715_m1
	HMGCR		3-hydroxy-3-methylglutaryl-CoA reductase	NM_002130.4:420	HS00153280_m1
	HMGCS1		3-hydroxy-3-methylglutaryl-CoA synthase 1 (soluble)	NM_001005291.1:1392	HS00892881_m1
	SREBF1		sterol regulatory element binding transcription factor 1	NM_004599.2:4080	HS00168966_m1
	SREBF2		sterol regulatory element binding transcription factor 2	NM_001129.3:250	HS00912671_m1
	SQLE		squalene epoxidase	NM_000384.2:2833	HS00925812_g1
	APOB		apolipoprotein B (including Ag(a) antigen)	NM_001645.3:270	HS00931443_m1
	APOC1		apolipoprotein C-I	NM_000041.2:96	HS01032443_m1
APOE		apolipoprotein E	NM_001861.2:160	HS00201955_m1	
Oxidative activity	COX4I1		cytochrome c oxidase subunit IV isoform 1	NM_004077.2:740	HS01042412_m1
	CS		citrate synthase	NM_00143.2:203	HS00950300_m1
	FH		fumarate hydratase	NM_002168.2:944	HS01037712_m1
	IDH2		isocitrate dehydrogenase 2 (NADP+), mitochondrial	NM_005917.3:970	HS00800172_s1
	MDH1		malate dehydrogenase 1, NAD (soluble)	NM_005918.2:475	HS00899690_m1
	MDH2		malate dehydrogenase 2, NAD (mitochondrial)	NM_002395.3:1405	HS00190006_m1
	ME1		malic enzyme 1, NAD(P)+-dependent, cytosolic	NM_002396.3:610	HS00853558_g1
	ME2		malic enzyme 2, NAD(P)+-dependent, mitochondrial	NM_001014811.1:1080	HS00195882_m1
	ME3		malic enzyme 3, NAD(P)+-dependent, mitochondrial	NM_002489.2:35	HS00195883_m1
	NDUFA4		NADH dehydrogenase (ubiquinone) 1 alpha subcomplex, 4, 9kDa	NM_002490.3:430	HS00601381_mH
	NDUFA6		NADH dehydrogenase (ubiquinone) 1 alpha subcomplex, 6, 14kDa	NM_004546.2:230	HS01072843_m1
	NDUFB2		NADH dehydrogenase (ubiquinone) 1 beta subcomplex, 2, 8kDa	NM_004547.4:254	HS00975961_g1
	NDUFB4		NADH dehydrogenase (ubiquinone) 1 beta subcomplex, 4, 15kDa	NM_002492.3:115	HS04260093_g1
	NDUFB5		NADH dehydrogenase (ubiquinone) 1 beta subcomplex, 5, 16kDa	NM_00199887.1:9	HS01027211_g1
	NDUFB6		NADH dehydrogenase (ubiquinone) 1 beta subcomplex, 6, 17kDa	NM_005005.2:80	HS01101235_g1
	NDUFB9		NADH dehydrogenase (ubiquinone) 1 beta subcomplex, 9, 22kDa	NM_00124054.1:1235	HS01081860_m1
	NDUFC2		NADH dehydrogenase (ubiquinone) 1, subcomplex unknown, 2, 14.5kDa	NM_002541.2:65	HS01085886_m1
	OGDH		oxoglutarate (alpha-ketoglutarate) dehydrogenase (lipoamide)	NM_000920.3:2055	HS00159918_m1
	PC		pyruvate carboxylase	NM_000925.3:555	HS00696862_m1
	PDHB		pyruvate dehydrogenase (lipoamide) beta	NM_001161778.1:950	HS00963166_m1
PDP1		pyruvate dehydrogenase phosphatase catalytic subunit 1	NM_020786.2:6505	HS00176883_m1	
PDP2		pyruvate dehydrogenase phosphatase catalytic subunit 2	NM_004168.1:230	HS01934174_s1	
SDHA		succinate dehydrogenase complex, subunit A, flavoprotein (Fp)	NM_005984.2:964	HS00831506_g1	
SLC25A1		solute carrier family 25 (mitochondrial carrier; citrate transporter), member 1	NM_012140.3:390	HS00159997_m1	
SLC25A10		solute carrier family 25 (mitochondrial carrier; dicarboxylate transporter), member 10	NM_003562.4:860	HS01015418_m1	
SLC25A11		solute carrier family 25 (mitochondrial carrier; oxoglutarate carrier), member 11	NM_178850.1:1116	HS00198333_m1	
Oxidative stress	HNF4A		hepatocyte nuclear factor 4, alpha	NM_0012289.3:561	HS01002566_m1
	KEAP1		kelch-like ECH-associated protein 1	NM_006164.4:746	HS00761782_s1
	NFE2L2/nrf2		nuclear factor (erythroid-derived 2)-like 2	NM_000454.4:35	HS00894603_m1
	SOD1		superoxide dismutase 1, soluble	NM_000636.2:640	HS01652468_g1
	SOD2		superoxide dismutase 2, mitochondrial	NM_003102.2:1135	HS01050510_s1
	SOD3		superoxide dismutase 3, extracellular	NM_019884.2:480	HS01380112_m1
	GSK3B		glycogen synthase kinase 3 beta	NM_002093.2:925	HS01682761_m1
	GSK3A		glycogen synthase kinase 3 alpha	NM_002567.2:1335	HS02561944_s1
	PEP1		phosphatidylethanolamine binding protein 1	NM_005542.3:1120	HS00192979_m1
	INSIG1		insulin induced gene 1	NM_016133.2:513	HS00417200_m1
Regulator of metabolism	INSIG2		insulin induced gene 2	NM_032951.2:2805	HS01562176_m1
	MLXIP1		MLX interacting protein-like	NM_004958.2:5095	HS00983079_m1
	MTOR		mechanistic target of rapamycin (serine/threonine kinase)	NM_002467.3:1610	HS04260081_mH
	MYC		y-myc myelocytomatosis viral oncogene homolog (avian)	NM_0012724.3:1080	HS01089954_m1
	NR1D1		nuclear receptor subfamily 1, group D, member 1	NM_007121.4:30	HS00537911_m1
	NR1H2		nuclear receptor subfamily 1, group H, member 2	NM_005693.2:1575	HS01056647_m1
	NR1H3		nuclear receptor subfamily 1, group H, member 3	NM_001001928.2:5220	HS01105604_g1
	PPARA		peroxisome proliferator-activated receptor alpha	NM_015869.3:1035	HS00201730_m1
	PPARG		peroxisome proliferator-activated receptor gamma	NM_006549.3:1710	HS03046298_s1
	CAMKK2		calcium/calmodulin-dependent protein kinase kinase 2, beta	NM_134442.2:200	HS04260091_mH
CREB1		cAMP responsive element binding protein 1	NM_013261.3:1505	HS01087948_g1	
PPARGC1A		peroxisome proliferator-activated receptor gamma, coactivator 1 alpha	NM_006623.3:1900	HS01046692_m1	
Serine/glycine synthesis	PHGDH		phosphoglycerate dehydrogenase	NM_021154.3:1445	HS01012127_g1
	PSAT1		phosphoserine aminotransferase 1	NM_004577.3:225	HS01001183_m1
	PSPH		phosphoserine phosphatase	NM_148918.1:1800	HS02330328_s1
	SHMT1		serine hydroxymethyltransferase 1 (soluble)	NM_001166356.1:1460	HS00533490_m1
	SHMT2		serine hydroxymethyltransferase 2 (mitochondrial)		

Pommier et al. Table S3 (Related to Figure 5)

List, abbreviations, accession numbers and Applied Bioscience references of the genes analyzed by Taqman assays in xenograft models.